THE ASTROPHYSICAL JOURNAL SUPPLEMENT SERIES, 112:391–414, 1997 October


# A SEARCH FOR "DWARF" SEYFERT NUCLEI. IV. NUCLEI WITH BROAD Hα EMISSION

LUIS C. HO[1] AND ALEXEI V. FILIPPENKO
Department of Astronomy, University of California, Berkeley, CA 94720-3411
WALLACE L. W. SARGENT
Palomar Observatory, 105-24 Caltech, Pasadena, CA 91125
AND
CHIEN Y. PENG
Department of Astronomy, University of California, Berkeley, CA 94720-3411
*Received 1997 January 9; accepted 1997 April 22*

## ABSTRACT

We present the results of an optical spectroscopic survey designed to search for low-luminosity "dwarf" Seyfert nuclei in a magnitude-limited ($B_T \leq 12.5$ mag) sample of 486 bright, northern galaxies. Moderate-resolution spectra of exceptionally high quality were obtained, in part to detect broad Hα emission similar in character to, but much weaker than, the broad permitted lines that define type 1 Seyfert nuclei. One of the primary goals of the survey is to better quantify the faint end of the luminosity function of active galactic nuclei.

This paper describes the subset of nuclei showing definite or probable evidence of broad Hα emission. We outline the procedures for determining the presence of this elusive spectral feature, steps for its quantitative measurement, and the associated systematic errors. Of the 211 emission-line galaxies classified as having Seyfert or LINER (low-ionization nuclear emission-line region) nuclei in our survey, the broad Hα line was detected with confidence in 34 objects and with less certainty in another 12. Most of the detections are reported for the first time, and the detection rate represents a lower limit to the true incidence of active nuclei harboring a broad emission-line region. These statistics imply that broad-lined active nuclei are much more common than previously believed: they exist in at least 20% of all galaxies spectroscopically classified as "active" and in more than 10% of all luminous galaxies at the current epoch.

Excluding nine well-known Seyfert 1 nuclei, the broad Hα lines of the remaining "dwarf" nuclei have median luminosity of $\sim 1 \times 10^{39}$ ergs s$^{-1}$ and median FWHM of $\sim 2200$ km s$^{-1}$. The broad lines constitute approximately 30% of the total emission of the Hα + [N II] λλ6548, 6583 blend. Several objects have broad Hα luminosities as low as (1–3) $\times 10^{38}$ ergs s$^{-1}$.

*Subject headings:* galaxies: active — galaxies: nuclei — galaxies: Seyfert — surveys

## 1. INTRODUCTION

Active galactic nuclei (AGNs) manifest themselves over a wide range of luminosities. Although the nuclei of Seyfert 1 galaxies have $L_B = 10^8$–$10^{11}$ $L_\odot$ ($M_B \approx -16$ to $-23$ mag: Weedman 1976), it is generally accepted that they present the same phenomenon as that associated with rare (at the present time) and more luminous QSOs whose power output is $L_B \approx 10^{11}$–$10^{14}$ $L_\odot$ ($M_B = -23$ to $-30$ mag: Schmidt & Green 1983). The basis for this belief rests on two main observational facts. On the one hand, Seyfert 1 nuclei and QSOs have very similar spectroscopic properties (Weedman 1976); on the other, it has become increasingly apparent that many low-redshift QSOs reside in structures photometrically resembling galaxies (Wyckoff et al. 1980; Malkan, Margon, & Chanan 1984; McLeod & Rieke 1994a, 1994b; Boyce et al. 1996; Bahcall et al. 1997), and spectroscopic confirmation that the extended nebulosities around QSOs come from starlight has been possible in some instances (Wyckoff et al. 1980; Boroson, Oke, & Green 1982; Balick & Heckman 1983; Miller, Tran, & Sheinis 1996).

The degree to which the AGN phenomenon extends to luminosities fainter than those of "classical" Seyferts has not yet been established. Several optical spectroscopic surveys of nearby galaxies (see Filippenko 1989 and Ho 1996 for reviews) corroborate that emission-line nuclei exhibiting excitation patterns indicative of nonstellar photoionization are quite common in the present epoch. The extensive survey recently completed by Ho, Filippenko, & Sargent (1995, hereafter Paper II), for example, revealed an astonishingly large population of galaxies with "active" nuclei: nearly half of all galaxies brighter than $B_T = 12.5$ mag can be classified as low-ionization nuclear emission-line regions (LINERs: Heckman 1980) or Seyfert galaxies (Ho 1995, 1996; Ho, Filippenko, & Sargent 1997b, hereafter Paper V). The nonstellar continuum and emission-line luminosities of these nuclei, however, can be orders of magnitude fainter than those of conventionally studied AGNs. The LINER/Seyfert nucleus of NGC 3031 (M81), for instance, has $M_B = -11.6$ mag and a broad Hα luminosity of only $1.8 \times 10^{39}$ ergs s$^{-1}$ (Ho, Filippenko, & Sargent 1996), while in the extreme case of NGC 4395, the Seyfert 1 nucleus has $M_B = -9.8$ mag and $L(\mathrm{H}\alpha) = 1.2 \times 10^{38}$ ergs s$^{-1}$ (Filippenko & Sargent 1989).

The exceptionally low luminosities of these sources have presented a serious observational challenge and have proven to be a major obstacle to furthering our understanding of them. Whether all the mildly "active" nuclei are low-power but genuine AGNs, and, if so, how they fit into the standard AGN paradigm remain outstanding unanswered questions. Particularly troublesome are LINERs,

[1] Present address: Harvard-Smithsonian Center for Astrophysics, 60 Garden Street, Cambridge, MA 02138.

which make up the bulk of the candidate AGNs, because their association with a nonstellar energy source is only one of several possible interpretations (Ho, Filippenko, & Sargent 1993; Filippenko 1996). The fundamental difficulty in determining the physical nature of low-luminosity AGNs stems from the extremely low contrast between the nucleus and the surrounding bulge. At optical wavelengths, the conventional telltale signs of AGN-related activity, such as the presence of a starlike nucleus, a blue, featureless continuum, or rapid variability, generally cannot be seen against the glare of the host galaxy. One possible exception may be the detection of broad emission lines. QSOs and luminous Seyfert 1 nuclei distinguish themselves unambiguously by their characteristic broad (full width at half-maximum [FWHM] of a few thousand kilometers per second) permitted lines (Khachikian & Weedman 1974). If such broad lines were to be found in low-luminosity AGNs, one could argue for an underlying physical connection between the two luminosity regimes. Since the strongest permitted line at optical wavelengths is expected to be H$\alpha$, searching for broad H$\alpha$ emission is a promising method of constraining the origin of the widespread nuclear activity found in spectroscopic surveys of nearby galaxies.

Weak, broad H$\alpha$ emission has long been known to be present in some nearby AGNs. Peimbert & Torres-Peimbert (1981), for example, noticed that the nucleus of NGC 3031 emits a broad H$\alpha$ line, and several other isolated cases have been noticed from time to time (see, e.g., Stauffer 1982; Keel 1983). Because of the formidable challenge in detecting this weak spectral feature, what has been lacking so far is a *systematic* study that can provide meaningful statistics on the incidence of broad H$\alpha$ emission. We have recently completed a survey aimed at achieving this goal. Using the Palomar 5 m Hale telescope, long-slit optical spectra were obtained of the nuclei of nearly 500 northern galaxies (Filippenko & Sargent 1985, hereafter Paper I). The sample is defined to be all galaxies listed in the Revised Shapley-Ames Catalog of Bright Galaxies (Sandage & Tammann 1981) with $\delta > 0°$ and $B_T \leq 12.5$ mag. Paper II presented the spectral atlas of the survey and discussed the observational parameters and data reduction, Ho, Filippenko, & Sargent (1997a, hereafter Paper III) gave the detailed line measurements and object classifications, and Paper V discussed the overall detection rates of the different classes of emission-line nuclei, their dependence on the host galaxy morphology and luminosity, and issues concerning completeness.

Here we summarize the overall properties of the subsample of emission-line nuclei showing broad H$\alpha$ emission. We describe the procedures necessary for confident determination of the presence of this weak, elusive spectral feature, steps for its quantitative measurement, and the associated systematic errors (§ 2). Plots of the data are provided for all candidates with positive detections, and (to illustrate our methods) for several others whose broad H$\alpha$ line is either more ambiguous or absent (§ 3). Section 4 discusses some of the overall implications of this work.

## 2. LINE DEBLENDING TECHNIQUES

### 2.1. *General Constraints*

A number of systematic effects plague the detection of faint, broad H$\alpha$ emission. The most serious of these is contamination from late-type stars, which dominate the integrated optical spectra of the centers of early-type spirals, the preferred hosts of active nuclei (see, e.g., Keel 1983; Paper V). As illustrated in Paper I, the continuum and spectral features of K and M giants can easily mimic a broad emission hump near the wavelength of H$\alpha$. Thus, detection of broad H$\alpha$, especially if weak, requires careful removal of the underlying starlight. Although this affects sources with strong broad H$\alpha$ emission less severely, quantitative measurements still require consideration of this effect. The details of the starlight subtraction for all the objects analyzed in this paper are given in Paper III.

For the line fitting procedure itself, it is necessary to impose some constraints in order to reduce the number of free parameters, as the H$\alpha$ + [N II] region (interchangeably called the "complex" in subsequent discussions) is generally quite complicated. In addition to a possible broad H$\alpha$ component, there are narrow lines of H$\alpha$ and of [N II] $\lambda\lambda$6548, 6583 that rarely show Gaussian profiles. The narrow lines generally have faint, extended wings near their bases, some degree of asymmetry, velocity blending among the three lines, and, occasionally, multiple velocity peaks. Any of these effects, alone or combined, can mimic or hide a broad H$\alpha$ component. Consequently, we have taken great care to examine all known systematic effects. Three methods, described below, were explored; each has its own merits and weaknesses depending on the object in question, and, in some cases, the final line parameters quoted were obtained by averaging the results of all three.

We assume that the H$\alpha$ and [N II] lines, and likewise the [S II] $\lambda\lambda$6716, 6731 lines, are separated by their laboratory wavelengths in the rest-frame spectra. The intensity ratio of [N II] $\lambda$6583/$\lambda$6548 is fixed at the theoretical value of 2.96, and we require that the two [N II] line profiles be identical. Since the [S II] doublet suffers from somewhat less confusion, in most cases a model for the narrow lines is derived from [S II]. (A different procedure is adopted for spectra whose signal-to-noise ratio [S/N] in the [S II] region is poor; see § 3.) We then use the model to deblend the more complicated H$\alpha$ + [N II] region, usually assuming that all the narrow lines have the same profile, but occasionally having to relax this constraint, especially for H$\alpha$. Although it is well known that the forbidden line in AGNs can have different profiles depending on their respective critical densities (Filippenko & Halpern 1984; Filippenko 1985; De Robertis & Osterbrock 1986), [N II] often has a line profile that closely matches that of [S II], despite having a significantly larger critical density (Filippenko & Halpern 1984; Filippenko 1985; Filippenko & Sargent 1988). Perhaps the [S II] and [N II] lines are dominated by emission from a relatively low-density reservoir of gas outside the stratified part of the narrow-line region.

### 2.2. *Automated Fitting*

The [S II] doublet can usually be fitted by a combination of several Gaussians, thereby yielding a set of analytic components that can then be applied to the narrow lines of H$\alpha$ and [N II]. The number of Gaussians for each of the [S II] lines, $N$, varies from 1 to as many as 4 or more, depending on the complexity of the profile. (Note that we do not necessarily ascribe physical significance to each individual Gaussian; this is merely a convenient fitting procedure.) Whenever possible, we make the first-order assumption that the components have the same intensity ratios for the two [S II] lines; this constraint must be relaxed in cases where

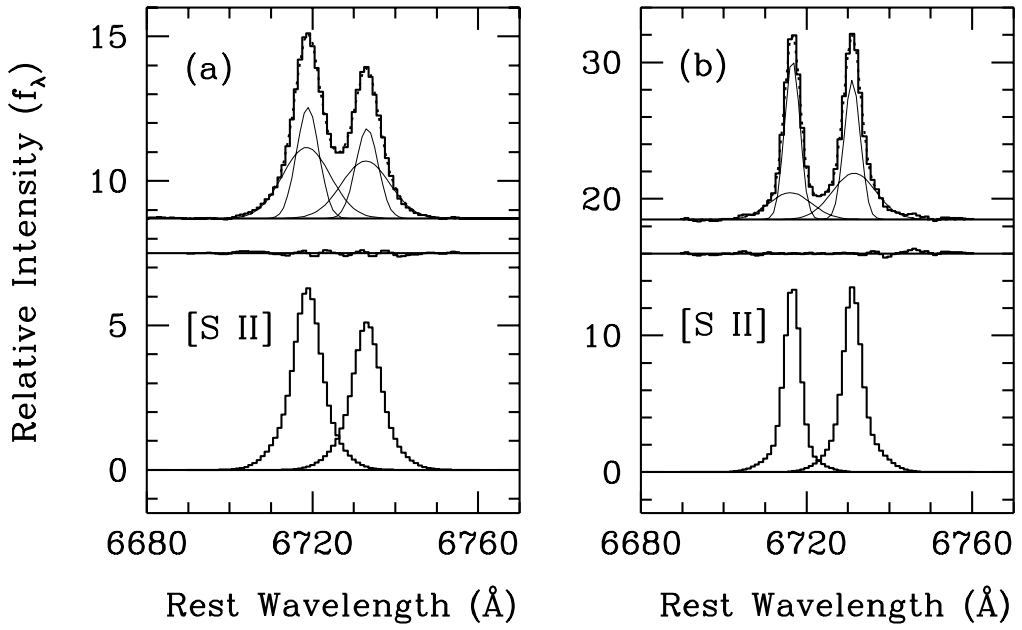


FIG. 1.—Decomposition of the [S II] $\lambda\lambda$6716, 6731 doublet for (*a*) NGC 4438 and (*b*) NGC 3031. Note that in NGC 4438, the two components used to model each line have the same intensity ratio, indicating that the electron density does not change with velocity. Each line in NGC 3031 can be modeled with two Gaussians, but the respective ratios for the two lines are not constant because of variations of the electron density with velocity. In all figures we have the following: *Histogram*, actual data; *solid curves*, individual components of the fit; *dotted curve*, final fit. *Top*: Spectra and Fits. *Bottom*: Model of each of the lines of the doublet.

the electron densities of the components are not similar. Figure 1 illustrates these two scenarios.

Once an [S II] model is derived, we fit the H$\alpha$ + [N II] complex using $3N + 1$ Guassians, $N$ components for each of the narrow lines and one component for broad H$\alpha$. As explained above, we force the [N II] lines to have identical profiles and a fixed intensity ratio, while the narrow component of H$\alpha$ is allowed to vary in its profile (but not in central wavelength) if necessary. Figure 2*a* shows an example of this procedure for the case of NGC 4278.

### 2.3. *Analytic and Synthetic Profile Scaling*

The broad H$\alpha$ profiles of some objects, notably most of the classical Seyfert 1 nuclei included in our sample, have highly irregular shapes that cannot be fitted with a single Gaussian. Imposing such a constraint would lead to clearly erroneous fits for the narrow lines, while increasing the number of Gaussian components to better match the broad line would allow too much freedom for the final solution of the narrow lines (at least when the broad and narrow components are not well separated). Under these circumstances, it is best simply to subtract appropriately scaled versions of the [S II] profile in order to remove the contribution of the narrow lines. We require that the [N II] lines have the correct intensity ratio and that the final broad H$\alpha$ profile be as smooth and continuous as possible. While this procedure is admittedly somewhat subjective, in some instances it offers the only practical solution.

The model [S II] profile can be obtained in two ways. The first method, hereafter referred to as "analytic profile scaling," is identical to that of the initial phase of "automated fitting"—namely, the best-fitting model for [S II] is obtained by finding a suitable combination of Gaussians (Fig. 2*b*). A second method, which we will call "synthetic profile scaling," constructs an empirical [S II] profile from the observed blend. As discussed by Filippenko & Sargent (1988), for example, a symmetric [S II] profile can be created by reflecting either the unblended blue half of the $\lambda$6716 line or the red half of the $\lambda$6731 line. Likewise, for

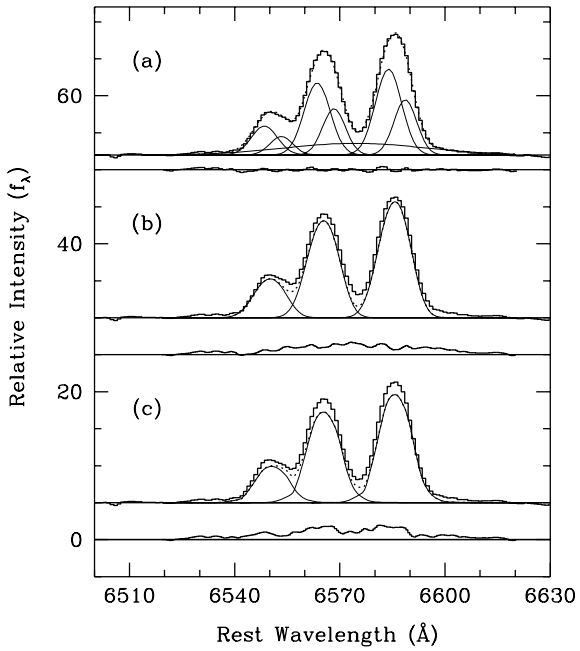


FIG. 2.—(*a*) Decomposition of the H$\alpha$ + [N II] region of NGC 4278 using the analytic narrow-line model obtained from [S II] $\lambda$6731. Each of the narrow lines, all of which are assumed to have identical profiles, is modeled by two Gaussians. We are able to extract a broad H$\alpha$ component with FWHM $\approx$ 1950 km s$^{-1}$ containing 19% of the flux of the total blend. (*b*, *c*). Same as (*a*), but using the methods of analytic and synthetic profile scaling.

obviously asymmetric lines, the blue half of $\lambda$6716 can be combined with the suitably scaled red half of the $\lambda$6731 line (Fig. 2*c*). Synthetic profile scaling can be easily implemented if the data have high S/N and if the [S II] lines are reasonably resolved; if the two [S II] lines severely overlap with each other, an iterative procedure can be attempted (see, e.g., Shields & Filippenko 1990), although the uniqueness of the resulting model profile then becomes difficult to ascertain.

### 2.4. *Uncertainties and Systematic Errors*

We performed simulations to gauge the reliability of our automated fitting procedure; of the three procedures described above, this one proved to be most useful for most of the survey. The tests were done using a high-S/N spectrum known in advance to have narrow lines with very similar profiles and to lack any visible broad H$\alpha$ emission, namely, the spectrum of NGC 7217. Next a grid of synthetic spectra was generated by introducing broad Gaussian components of various widths and amplitudes centered at the wavelength of H$\alpha$. To better represent the average quality of the data, we added Poisson noise to the spectra, and we introduced small fluctuations of random amplitude and frequency to the continuum level to mimic imperfections that might arise from the starlight subtraction process. We parameterized the broad emission line with FWHM = 20, 40, 60, and 80 Å and $f_{\rm blend}$ = 10%, 20%, 40%, 60%, and 80%, where $f_{\rm blend}$ is the fraction of the flux in the H$\alpha$ + [N II] complex contributed by the broad H$\alpha$ line; these values of the FWHM and of $f_{\rm blend}$ roughly bracket the range of values actually measured in the survey galaxies. We then constructed a model from the [S II] doublet and attempted to recover the broad H$\alpha$ line.

The results of these simulations (Fig. 3*a*) indicate that the input FWHM and $f_{\rm blend}$ parameters of the broad H$\alpha$ line can be recovered to within $\sim$10%, provided that FWHM $\gtrsim$ 10 Å and $f_{\rm blend} \gtrsim 20\%$ if the spectral resolution at H$\alpha$ is assumed to be 2.5 Å, the nominal value for our survey. As to be expected, for a fixed line width, the errors become progressively larger when the broad line has low contrast with respect to the H$\alpha$ + [N II] blend ($f_{\rm blend}$ small). Conversely, for a fixed relative line strength, it is more difficult to recover a line with a larger breadth because it becomes increasingly washed out into the continuum. So long as the [S II], H$\alpha$ and [N II] lines have similar profiles, and provided that the S/N of the data, the quality of the starlight subtraction, and the spectral resolution are relatively high (i.e., comparable to those of our survey), we believe that our method can reliably extract a weak broad H$\alpha$ component with FWHM $\approx$ 1000–3000 km s$^{-1}$ even if it comprises only about 20% of the flux of the H$\alpha$ + [N II] blend. From the H$\alpha$ line fluxes and [N II]/H$\alpha$ ratios reported in Paper III, the typical H$\alpha$ + [N II] blend for the AGNs in our sample has a flux of $\sim 3 \times 10^{-14}$ ergs s$^{-1}$ cm$^{-2}$; thus we conservatively estimate that our flux detection limit for the broad H$\alpha$ line is $\sim 6 \times 10^{-15}$ ergs s$^{-1}$ cm$^{-2}$. This corresponds to an H$\alpha$ luminosity of $3 \times 10^{38}$ ergs s$^{-1}$ for the median distance of 20.6 Mpc for the AGN sample (Paper V). In a few cases (e.g., NGC 4388, in § 3), even fainter levels can be detected.

For the benefit of workers who may only have access to data of lower spectral resolution, we repeated the simulations on spectra that were degraded to a resolution (at H$\alpha$) of 5 Å (Fig. 3*b*) and 10 Å (Fig. 3*c*). Not surprisingly, the errors are larger in these cases, but evidently it is still possible to detect broad H$\alpha$ under most conditions, provided, of course, that the data have sufficiently high S/N and that starlight subtraction has been taken properly into account.

In some circumstances, discussed in detail where relevant in § 3, our techniques of profile fitting do not lead to unique solutions. Moreover, the broad H$\alpha$ fluxes derived for a few objects can differ by large factors ($\sim$2) depending on the technique used, and it is not always clear which of these is the most reliable. This problem most severely affects objects with a weak broad-line component.

One of the most important potential sources of systematic error stems from the assumptions made during the line-fitting process concerning the intrinsic profiles of the narrow components of H$\alpha$ and [N II]. We always begin with the conservative and empirically supported (see, e.g., Filippenko & Halpern 1984; Filippenko 1985; Filippenko & Sargent 1988) hypothesis that the profiles of these lines can be approximated by that of at least one of the [S II] lines. If all or most low-luminosity AGNs obey a strict line width versus critical density relation, [N II] should have a broader profile than [S II]. Although this result appeared not to hold in the few objects analyzed in the above-mentioned studies, it should be noted that minor differences in the widths of the *wings* of the narrow lines would have escaped notice in the objects examined. In the case of NGC 3031 (see § 3 and Filippenko & Sargent 1988), for instance, the broad component of H$\alpha$ is sufficiently strong and non-Gaussian in shape that it would be difficult to perceive subtle mismatches between the profiles of narrow H$\alpha$, [N II], and [S II]. Indeed, as described in § 3, profile differences among these three lines clearly exist in some objects. An alternative strategy might be to use, instead, [O III] $\lambda$5007 as the model. However, this does not alleviate the difficulty, since the critical density of [O III] is larger than that of [N II]; moreover, although [O III] is usually quite strong, the blue spectra in our survey have lower spectral resolution (by about a factor of 2) and generally lower S/N than the red spectra.

Although the profiles of narrow H$\alpha$ and [N II] closely match each other in the majority of objects, exceptions do exist. These can arise in one of two ways. First, the height, and hence the width, of the narrow component of H$\alpha$ emission critically depends on the accuracy with which the underlying H$\alpha$ absorption line has been removed during the process of starlight subtraction. Second, genuine profile differences *do* exist in objects with composite nuclei (e.g., NGC 4303: Paper I). Mixing an H II region component with an AGN component changes the line profiles of the two lines because the [N II]/H$\alpha$ ratio differs for the two excitation mechanisms.

Another source of uncertainty may enter through errors in the determination of the spectrograph response function, which directly affects the derived continuum shape. In general, the response function for our data is known quite accurately, as judged by the calibrated continuum energy distributions of the standard stars observed along with the program galaxies. However, temporal variations in the spatial focus of the spectrograph, which can introduce low-frequency flux undulations in the spectra, occasionally plagued some of our data, particularly those taken with the red CCD camera. As discussed in Paper II, we made great efforts to rectify this problem during the calibration process,

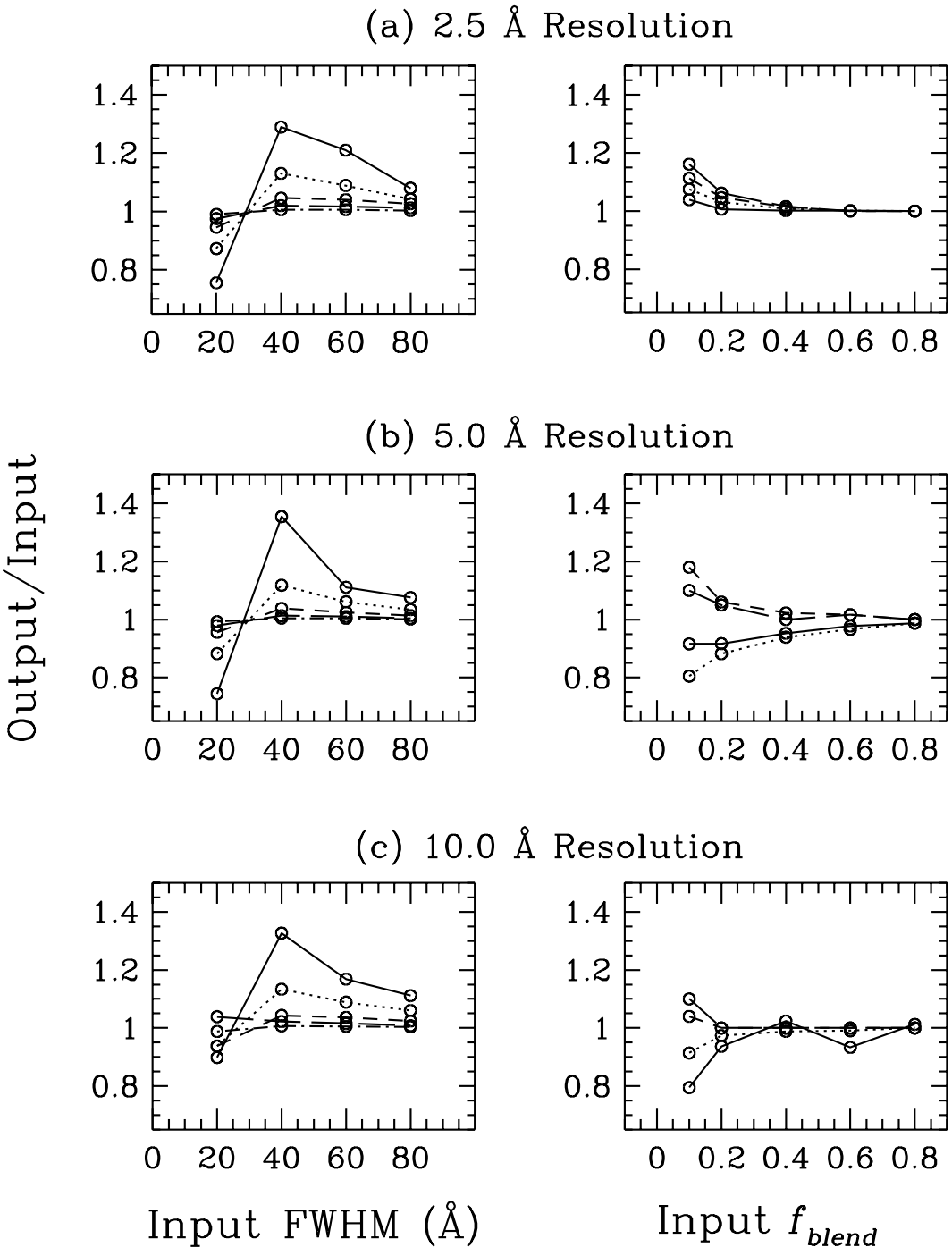


FIG. 3.—Simulations of our automated fitting procedure to search for broad Hα (see § 2.4 for details). (*a*) Broad Hα components with several values of FWHM and $f_{blend}$ were added to the high-S/N, narrow-lined spectrum of NGC 7217 having a spectral resolution of 2.5 Å at Hα. *Left*: Fraction of the FWHM recovered as a function of FWHM and $f_{blend}$. The solid, dotted, short-dashed, long-dashed, and dot-dashed lines correspond to $f_{blend}$ = 10%, 20%, 40%, 60%, and 80%, respectively. *Right*: fraction of $f_{blend}$ recovered as a function of $f_{blend}$ and FWHM. The solid, dotted, short-dashed, and long-dashed lines correspond to FWHM = 20, 40, 60, and 80 Å, respectively. (*b*, *c*) Same as (*a*), but for spectral resolutions of 5.0 and 10.0 Å, respectively.

and we believe that the broad Hα measurements in this paper should not be adversely affected.

Finally, systematic errors can enter during the starlight subtraction phase of the data analysis. Mismatch of the overall continuum shape between the object spectrum and the absorption-line template, such as might arise from imperfect calibration, differences in reddening, or a true discrepancy in the stellar population, will result in artificial structure in the residual emission-line spectrum. Our procedure for the starlight subtraction (Paper III), however, explicitly removes any gross differences in the general continuum shape between the object and the template. An imperfect fit of the stellar population can also introduce, in one of two ways, a discrete feature mimicking broad Hα emission. First, as already mentioned in § 2.1, the continuum of late-type giant stars exhibits a broad maximum near the wavelength of Hα (see Fig. 12 of Paper I) that can easily be mistaken for a broad Hα emission line. Our starlight

subtraction should be sufficiently accurate that this effect is probably minor. Second, if the underlying stellar population has a significant contribution from A-type stars, it is possible to generate an artificial "bump" resembling broad Hα emission. Since the wings of the Balmer absorption lines in most subclasses of A stars are widened considerably by pressure broadening, oversubtraction of the A-star component in the template spectrum results in a broad peak centered at the expected position of each Balmer line. Similarly, undersubtraction generates a negative depression (or "bowl") in the local continuum surrounding the Balmer emission line. These signatures are easily observable at Hβ, where blending with neighboring emission lines is rarely an issue. Since, in our sample, genuine broad Hβ emission is not observed except in the previously known Seyfert 1 nuclei and in a small number of the brightest other Seyfert 1 nuclei, the flatness of the local continuum near Hβ serves as an excellent gauge of how well the young stellar population has been removed (see also discussion in Paper III).

In the next section we try to fold these complications, which are difficult to quantify rigorously, into our evaluation of the presence or absence of broad Hα emission.

## 3. RESULTS

Here we summarize the results of the profile fitting. All objects with definite or probable detections of broad Hα are discussed individually, with the accompanying fits shown to convey the maximum amount of information. To illustrate some technical issues, we also show a number of examples of null detections. Table 1 summarizes several parameters of interest for the objects in which broad Hα has been definitely or probably detected. Note that the parameters of the broad Hα line given in Table 1 refer only to observations taken at a single epoch. Several objects are known to show variable broad-line emission, and these are highlighted below. In a few objects, mainly the well-known Seyfert 1 nuclei in the sample, a broad component is easily visible in permitted lines other than Hα, and we point these out accordingly.

*NGC 266.*—A broad Hα component is obvious even before profile decomposition, as evidenced by the extra "bump" between narrow Hα and [N II] λ6583 (Fig. 4*a*). Since the rather noisy [S II] region could not be fitted to give a reliable model for the narrow lines, we resorted to fitting the Hα + [N II] complex independently. Each of the narrow lines required two components, as they are each slightly asymmetric to the blue, but we forced all three lines to have identical profiles. The resulting narrow-line profile, when applied to the [S II] lines, provided a reasonable fit. The broad Hα line, with FWHM ≈ 1350 km s$^{-1}$ and $f_{\rm blend} \approx 30\%$, appears to be redshifted by ∼350 km s$^{-1}$ with respect to the narrow component of Hα. The latter effect may be an artifact of the uncertain continuum level, as the negative dip shortward of [N II] λ6548 probably influences the derived central wavelength of the broad Hα feature.

*NGC 315.*—As noted previously by Ho et al. (1993), a broad Hα component is present in this radio galaxy with twin radio jets (Giovannini, Feretti, & Comoretto 1989), but its strength turns out to be considerably weaker ($f_{\rm blend} \approx 29\%$) than what might be perceived by eye (Fig. 4*b*). The narrow lines have very broad, non-Gaussian wings, easily discernible, for instance, in the [S II] lines. Unfortunately, the model for the [S II] lines is not well determined because [S II] λ6731 is partly redshifted out of our spectral range.

*NGC 660.*—This transition object (LINER + H II nucleus) may contain extremely weak broad Hα emission, but its reality is suspect because of a possible template mismatch. As the narrow lines have unusually small widths (FWHM ≈ 200 km s$^{-1}$), very faint emission between Hα and [N II] is discernible. When fitted with a single Gaussian, the broad component appears to contain about 8% of the total flux of the blend (Fig. 4*c*).

*NGC 841.*—The [S II] lines are too noisy to provide a reliable model; however, the narrow lines of Hα and [N II] are fairly symmetric and can be fitted with single Gaussians. A four-component fit to the complex (Fig. 4*d*) reveals a sizable broad Hα line ($f_{\rm blend} \approx 39\%$). The continuum surrounding the line complex unfortunately has large residuals, making the fit somewhat uncertain.

*NGC 1052.*—This historically important object inspired much of the early discussion on the relative contribution of shocks and photoionization to the excitation of LINERs (Fosbury et al. 1978; Keel & Miller 1983; Rose & Tripicco 1984). We confirm the presence of broad Hα emission ($f_{\rm blend} \approx 32\%$; FWHM ≈ 1950 km s$^{-1}$) suspected in Paper I. The evident asymmetry of the narrow lines and the substantial rotational broadening (FWHM ≈ 480 km s$^{-1}$), conspire to make the fitting rather tricky. Nevertheless, a reasonably good fit can be achieved using the model derived from the [S II] lines (Fig. 4*e*), and all three fitting methods give consistent results for the broad Hα flux. The detection of broad Hα furnishes strong evidence that the nucleus of NGC 1052 should indeed be regarded as active.

*NGC 1068.*—Malkan & Filippenko (1983) first remarked that the Seyfert nucleus of NGC 1068 may have weak broad Hβ emission, although they did not explicitly model the line profile to measure the broad line. The existence of a broad-line region (BLR) in this object was subsequently demonstrated conclusively by Antonucci & Miller (1985), whose spectropolarimetric observations showed that the polarized spectrum closely resembled that of a typical Seyfert 1 nucleus. Here we wish to reexamine whether the broad component of Hβ and Hα can be detected in the total-light spectrum. The kinematics and spatial distribution of the narrow-line region in NGC 1068 are notoriously complicated. It has long been known that the line-emitting material within the central several hundred parsecs consists of a number of distinct, high-velocity clumps (Walker 1968) that combine to produce very complex, exceptionally broad line profiles (see, e.g., Pelat & Alloin 1980), that the integrated line profile changes dramatically over small angular scales (see, e.g., Alloin et al. 1983; Baldwin, Wilson, & Whittle 1987), and that the line-intensity ratios of the different velocity components do not remain constant throughout the nuclear region (Baldwin et al. 1987; Cecil, Bland, & Tully 1990). Thus, we anticipate at the outset that many of the assumptions employed thus far in this study are unlikely to be applicable in NGC 1068.

We begin with the Hβ line, since it is much less blended with surrounding lines than Hα is. Although the profiles of Hβ and [O III] differ in detail, previous studies indicate that these two lines roughly trace each other in overall shape (see, e.g., Cecil et al. 1990; Veilleux 1991), especially as seen in data with moderate spectral resolution. We therefore constrain the narrow component of Hβ to have the same profile as that of [O III]. An additional Gaussian was then introduced to test for the presence of possible broad Hβ emission. We leave the height of the Gaussian uncon-

TABLE 1

GALAXIES WITH BROAD Hα EMISSION

| Galaxy (1) | Class (2) | Hα + [N II] (3) | $f_{blend}$ (4) | $f_{H\alpha}$ (5) | FWHM (6) | log $F(H\alpha)_b$ (7) | log $L(H\alpha)_b$ (8) | Notes (9) |
|---|---|---|---|---|---|---|---|---|
| NGC 266 ..... | L1.9 | 7.34 | 0.30 | 0.64 | 1350 | −14.11 | 39.56 | 1 |
| NGC 315 ..... | L1.9 | 13.23 | 0.29 | 0.67 | 2000 | −13.86 | 39.85 | 1 |
| NGC 841 ..... | L1.9: | 13.88 | 0.39 | 0.65 | 1350 | ... | ... | 2 |
| NGC 1052..... | L1.9 | 6.11 | 0.32 | 0.55 | 1950 | ... | ... | 1 |
| NGC 1068..... | S1.8 | 12.29 | 0.13 | 0.24 | 3210 | ... | ... | 2, 3 |
| NGC 1161..... | T1.9: | 17.47 | 0.29 | 0.58 | 3000 | −14.07 | 38.83 | 1 |
| NGC 1275..... | S1.5 | 14.13 | 0.59 | 0.79 | 2750 | −11.97 | 41.79 | 1 |
| NGC 2639..... | S1.9 | 27.66 | 0.17 | 0.58 | 3100 | ... | ... | 1 |
| NGC 2681..... | L1.9 | 20.39 | 0.33 | 0.67 | 1550 | ... | ... | 1 |
| NGC 2787..... | L1.9 | 6.18 | 0.35 | 0.63 | 2050 | −13.55 | 38.76 | 1 |
| NGC 2985..... | T1.9 | 4.61 | 0.22 | 0.37 | 2050 | ... | ... | 2 |
| NGC 3031..... | S1.5 | 9.52 | 0.57 | 0.86 | 2650 | −12.02 | 39.17 | 1, 4 |
| NGC 3226..... | L1.9 | 6.18 | 0.34 | 0.60 | 2000 | −13.73 | 39.09 | 1 |
| NGC 3227..... | S1.5 | 7.82 | 0.71 | 0.87 | 2950 | ... | ... | 1 |
| NGC 3516..... | S1.2 | 6.54 | 0.91 | 0.97 | 3850 | ... | ... | 1 |
| NGC 3642..... | L1.9 | 6.26 | 0.35 | 0.51 | 1250 | ... | ... | 1 |
| NGC 3718..... | L1.9 | 9.32 | 0.50 | 0.68 | 2350 | ... | ... | 1 |
| NGC 3884..... | L1.9 | 10.74 | 0.19 | 0.47 | 2100 | −13.76 | 40.24 | 2 |
| NGC 3982..... | S1.9 | 10.89 | 0.12 | 0.23 | 2150 | −13.85 | 38.69 | 2 |
| NGC 3998..... | L1.9 | 11.51 | 0.37 | 0.59 | 2150 | −12.58 | 40.16 | 1 |
| NGC 4036..... | L1.9 | 11.43 | 0.14 | 0.39 | 1850 | −13.69 | 39.17 | 2 |
| NGC 4051..... | S1.2 | 6.13 | 0.74 | 0.84 | 1000 | ... | ... | 1 |
| NGC 4138..... | S1.9 | 10.86 | 0.23 | 0.47 | 1650 | −14.05 | 38.49 | 2 |
| NGC 4143..... | L1.9 | 5.42 | 0.45 | 0.74 | 2100 | −13.41 | 39.13 | 1 |
| NGC 4151..... | S1.5 | 6.49 | 0.63 | 0.77 | 3250 | ... | ... | 1 |
| NGC 4168..... | S1.9: | 8.97 | 0.52 | 0.84 | 2850 | −14.21 | 38.32 | 1 |
| NGC 4203..... | L1.9 | 3.58 | 0.34 | 0.64 | 1500 | −13.46 | 38.59 | 1 |
| NGC 4235..... | S1.2 | 34.65 | 0.84 | 0.96 | 7600 | −12.56 | 40.61 | 1 |
| NGC 4258..... | S1.9 | 8.16 | 0.49 | 0.67 | 1700 | −13.09 | 38.65 | 1 |
| NGC 4278..... | L1.9 | 6.55 | 0.19 | 0.38 | 1950 | −13.07 | 38.98 | 1 |
| NGC 4388..... | S1.9 | 10.04 | 0.02 | 0.04 | 3900 | ... | ... | 1 |
| NGC 4395..... | S1.8 | 3.36 | 0.63 | 0.73 | 442 | −12.83 | 38.08 | 1, 5 |
| NGC 4438..... | L1.9 | 18.07 | 0.09 | 0.24 | 2050 | −13.64 | 38.89 | 2 |
| NGC 4450..... | L1.9 | 9.20 | 0.20 | 0.48 | 2300 | ... | ... | 2 |
| NGC 4565..... | S1.9 | 21.33 | 0.16 | 0.45 | 1750 | −14.15 | 37.89 | 2 |
| NGC 4579..... | S1.9 | 10.91 | 0.21 | 0.48 | 2300 | −13.08 | 39.45 | 1 |
| NGC 4636..... | L1.9 | 9.19 | 0.27 | 0.56 | 2450 | −14.18 | 38.36 | 1 |
| NGC 4639..... | S1.0 | 7.96 | 0.90 | 0.96 | 3600 | −12.83 | 39.70 | 1 |
| NGC 4750..... | L1.9 | 15.82 | 0.17 | 0.50 | 2200 | −13.85 | 39.06 | 1 |
| NGC 4772..... | L1.9 | 8.74 | 0.38 | 0.63 | 2400 | ... | ... | 1 |
| NGC 5005..... | L1.9 | 19.62 | 0.33 | 0.79 | 1650 | −12.69 | 40.05 | 1 |
| NGC 5033..... | S1.5 | 18.57 | 0.50 | 0.81 | 2850 | −12.69 | 39.94 | 1 |
| NGC 5077..... | L1.9 | 7.42 | 0.12 | 0.26 | 2300 | −14.06 | 39.23 | 2 |
| NGC 5273..... | S1.5 | 8.05 | 0.84 | 0.93 | 3350 | ... | ... | 1 |
| NGC 5548..... | S1.5 | 3.03 | 0.96 | 0.98 | 4200 | ... | ... | 1 |
| NGC 7479..... | S1.9 | 22.01 | 0.08 | 0.19 | 2250 | −14.18 | 38.92 | 2 |

NOTES.—Col. (1): Galaxy name. Col. (2): Classification of nucleus (see Paper III), where L = LINER, T = transition object (LINER/H II nucleus), S = Seyfert, 1 = type 1, 2 = type 2, and a fractional number between 1 and 2 denotes various intermediate types; entries followed by a colon denote uncertain or ambiguous classification of the narrow-line spectrum. Col. (3): Intensity of the Hα + [N II] λλ6548, 6583 blend relative to the narrow component of Hβ. Col. (4): Fractional contribution of the broad component of Hα to the Hα + [N II] blend. Col. (5): Fractional contribution of the broad component of Hα to the total (broad + narrow) Hα emission. Col. (6): FWHM of broad Hα in units of km $s^{-1}$. Col. (7): Observed (not corrected for reddening) flux of broad Hα in units of ergs $s^{-1}$ $cm^{-2}$ (fluxes given only for objects observed under photometric conditions). Col. (8): Observed (not corrected for reddening) luminosity of broad Hα in units of ergs $s^{-1}$, assuming distances adopted in Paper III. Col. (9): (1) Definite detection of broad Hα emission. (2) Probable detection of broad Hα emission. (3) FWHM fixed. (4) Flux and distance taken from Ho et al. 1996. (5) Flux and distance taken from Filippenko & Sargent 1989.

strained but fix the FWHM to be 3210 km $s^{-1}$ and the line center redshifted by 600 km $s^{-1}$ with respect to the narrow component; these parameters, taken from the spectropolarimetric study of Miller, Goodrich, & Mathews (1991), pertain to the polarized broad Hβ profile from the nucleus and should be identical to that of the hypothetical component viewed in total light. We cannot allow too much freedom in the fit for the broad component because the extended bases of the narrow lines, especially the blue wing anticipated from [O III] λ4959, can easily lead to an erroneous, even if formally acceptable, solution. Our best-fit model for each of the [O III] lines (Fig. 5*a*) consists of a sum of five Gaussians: four have FWHM ≈ 400–600 km $s^{-1}$ and contain about half of the flux and another is considerably broader (FWHM ≈ 1900 km $s^{-1}$) and slightly blueshifted (∼190 km $s^{-1}$) relative to the main narrow component. The broad, blueshifted feature identified here most likely corresponds to a similar component seen in many previous studies (see, e.g., Pelat & Alloin 1980; Alloin et al. 1983; Caganoff et al. 1991) and lends confidence that our model for the narrow lines is qualitatively correct. Under this assumption, the fit for the Hβ line *does* require

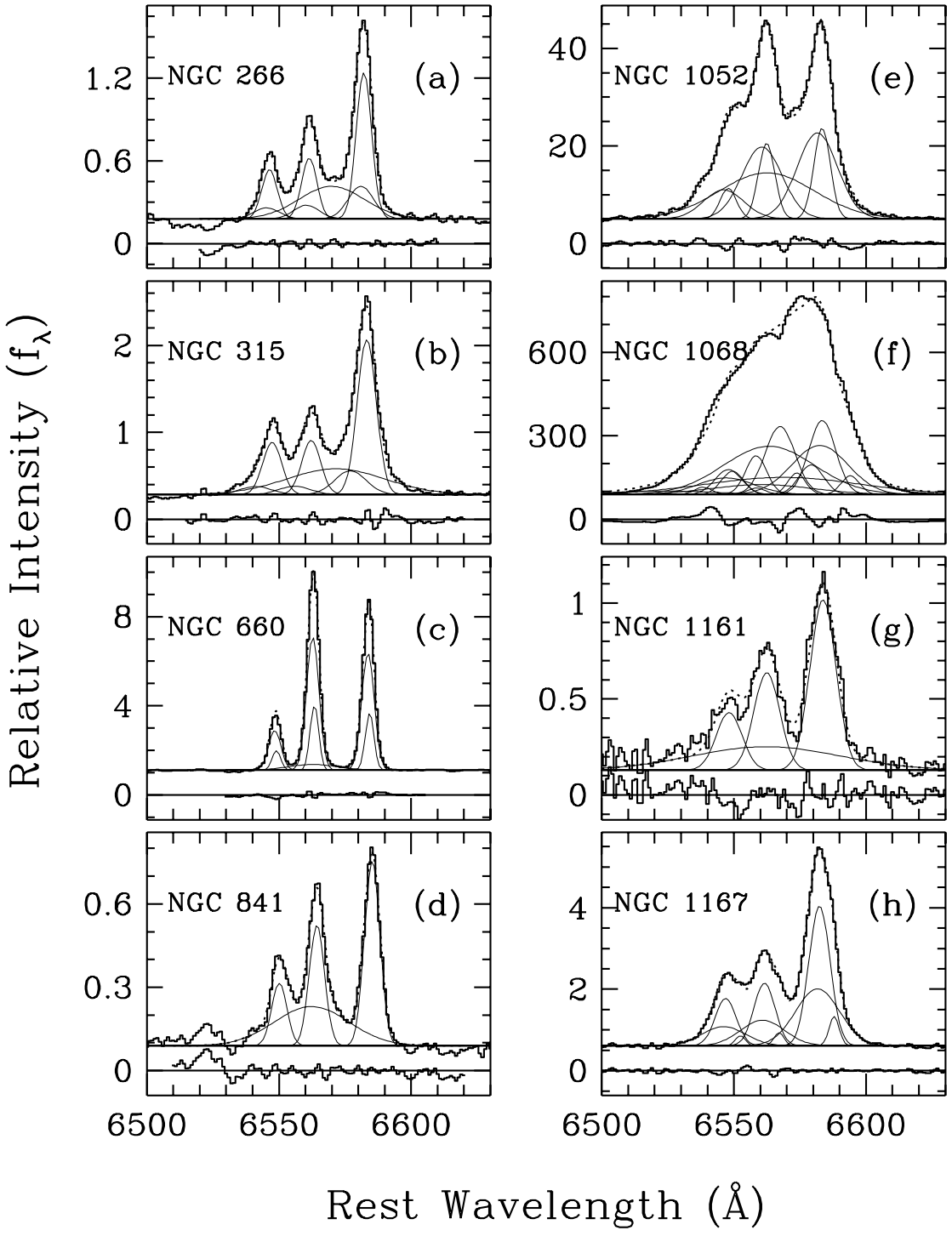


FIG. 4.—Decomposition of the Hα + [N II] region for (*a*) NGC 266, (*b*) NGC 315, (*c*) NGC 660, (*d*) NGC 841, (*e*) NGC 1052, (*f*) NGC 1068, (*g*) NGC 1161, and (*h*) NGC 1167.

a BLR component (*bottom*, Fig. 5*a*). Interestingly, the broad Hβ line has roughly the strength expected from the detailed model by Miller et al. for the scattered line flux of the nucleus. The broad line we detect constitutes ∼19% of the integrated flux of Hβ, and it has 1.8% of the total intensity of [O III] λ5007. Although our observations of this source were not taken under photometric conditions, we can estimate the flux of the broad Hβ line as follows. Assuming, as did Miller et al., that the flux of [O III] λ5007 is $1.7 \times 10^{-11}$ ergs $s^{-1}$ $cm^{-2}$ (Shields & Oke 1975), the flux of broad Hβ should be $3.1 \times 10^{-13}$ ergs $s^{-1}$ $cm^{-2}$, in very close agreement with the value of $3.7 \times 10^{-13}$ ergs $s^{-1}$ $cm^{-2}$ estimated by Miller et al.

The Hα + [N II] region is considerably more complicated. In addition to the severe blending of the broad, complex lines, it appears that the intrinsic narrow-line profile of Hα does not match that of [N II]. If we construct an analytic model from [S II] as usual (Fig. 5*b*), it is evident that the [S II] lines have a much more extended blue tail than [O III]; a broad component is again evident (FWHM ≈ 2050 km $s^{-1}$), but it is significantly more blueshifted (∼1000 km $s^{-1}$). Thus, a priori, we expect that

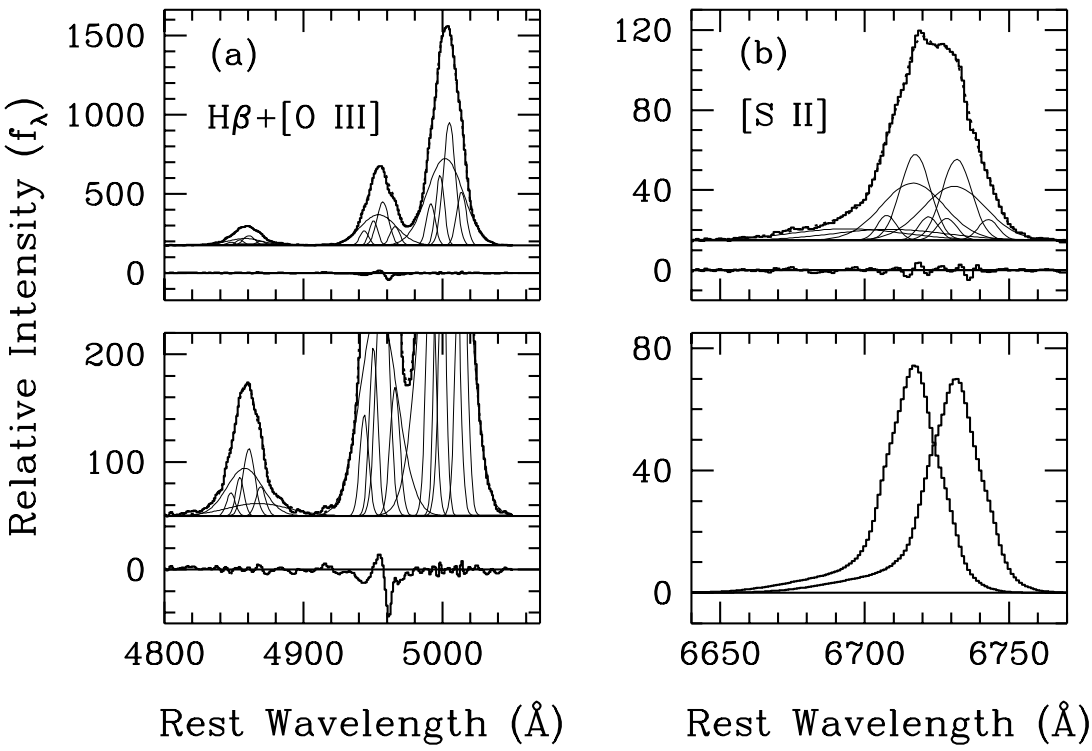


FIG. 5.—(*a*) Decomposition of the H$\beta$ + [O III] $\lambda\lambda$4959, 5007 region for NGC 1068. *Top*, Full scale spectrum; *bottom*, expanded view. The profile of narrow H$\beta$ was constrained to be identical to that of the [O III] lines, each of which is represented by five Gaussians, and an additional Gaussian was introduced to model broad H$\beta$. We fixed the FWHM of the broad component of H$\beta$ to be 3210 km s$^{-1}$ and its centroid to be redshifted by 600 km s$^{-1}$ with respect to the narrow component. (*b*) Decomposition of the [S II] $\lambda\lambda$6716, 6731 region for NGC 1068. *Top*: Original data and the individual Gaussian components (five for each line). *Bottom*: Summed model profiles.

making the assumption that the profiles of [S II], [N II], and H$\alpha$ are equal is invalid, since H$\beta$, which presumably should be nearly identical to H$\alpha$, is well fitted by [O III]. On the other hand, we find that [O III] clearly does not match [N II], whereas [S II] approximately does. Accordingly, we constructed a model such that H$\alpha$ and [O III] had identical profiles and [N II] and [S II] had identical profiles, and we once again added an extra Gaussian to test for the presence of broad H$\alpha$ emission. As in the case of H$\beta$, we fixed the position and the width of the Gaussian. Under these assumptions, we *also* find evidence for a BLR component of H$\alpha$ (Fig. 4*f*). Although the fairly large residuals indicate that our fit is far from perfect, omitting the BLR component results in much larger residuals. As with the BLR component of H$\beta$, the broad H$\alpha$ line contains $\sim$20% of the total flux of H$\alpha$, and it has a sensible strength—the ratio of broad H$\alpha$ to broad H$\beta$ is 7, close to values typically seen in Seyfert 1 nuclei (see, e.g., Netzer 1990).

To summarize, our profile analysis suggests that both the H$\alpha$ and the H$\beta$ emission lines display a broad component in the total-light spectrum. We believe that this broad component arises from the BLR and is distinct from the high-velocity emission associated with the narrow-line region. Our measurement of this component, however, is by no means straightforward, and because of the simplifying assumptions that had to be adopted, we cannot be sure that our profile fits are unique. Nevertheless, it is encouraging that the derived strength of the broad H$\beta$ line agrees so well with the predictions of the Miller et al. (1991) model and that the results of the H$\alpha$ fit are consistent with those of the H$\beta$ fit. It is of historical interest to note that, based on these results, NGC 1068 technically should *not* be classified as a Seyfert galaxy of type 2 but, rather, as one of type 1.8 (weak broad H$\alpha$ and H$\beta$: Osterbrock 1981).

*NGC 1161.*—Despite the poor S/N of the data, a broad component of H$\alpha$ can be seen clearly in the starlight-subtracted spectrum even without profile fitting (Fig. 4*g*). We obtained the final fit by repeated trials in which both the FWHM and central wavelength of the broad component were fixed at different input values while the height of the broad-component and the parameters of the narrow lines were varied.

*NGC 1167.*—The presence of faint wings near the base of the [N II] lines led us to suspect, in Paper I, that broad H$\alpha$ might be present in NGC 1167. However, similar wings can be seen in the [S II] profiles, and a careful fit of the H$\alpha$ + [N II] blend indicates that broad H$\alpha$ is not present (Fig. 4*h*).

*NGC 1275.*—As discussed in Paper I, the broad H$\alpha$ component of NGC 1275 has extremely wide wings. In addition to the narrow lines' unusually large breadth (FWHM $\approx$ 450 km s$^{-1}$ for [N II] and [S II]), they also have quite extended wings, making decomposition difficult. Nevertheless, each [S II] line can be represented by three Gaussians, the sum of which was then used to remove the narrow lines from the complex by analytic profile scaling (Fig. 6*a*); repeating the process using synthetic profile scaling gave virtually identical results. The final broad H$\alpha$ line has FWHM $\approx$ 2750 km s$^{-1}$, full width near zero intensity (FWZI) $\sim$ 19,000 km s$^{-1}$, and contains 59% of the flux of the entire blend. A broad component has also been detected in H$\beta$, H$\gamma$, and He II $\lambda$4686.

*NGC 1358.*—This object provides an excellent illustration of the potential ambiguities and limitations of our method. If we make the usual assumption that the [S II]

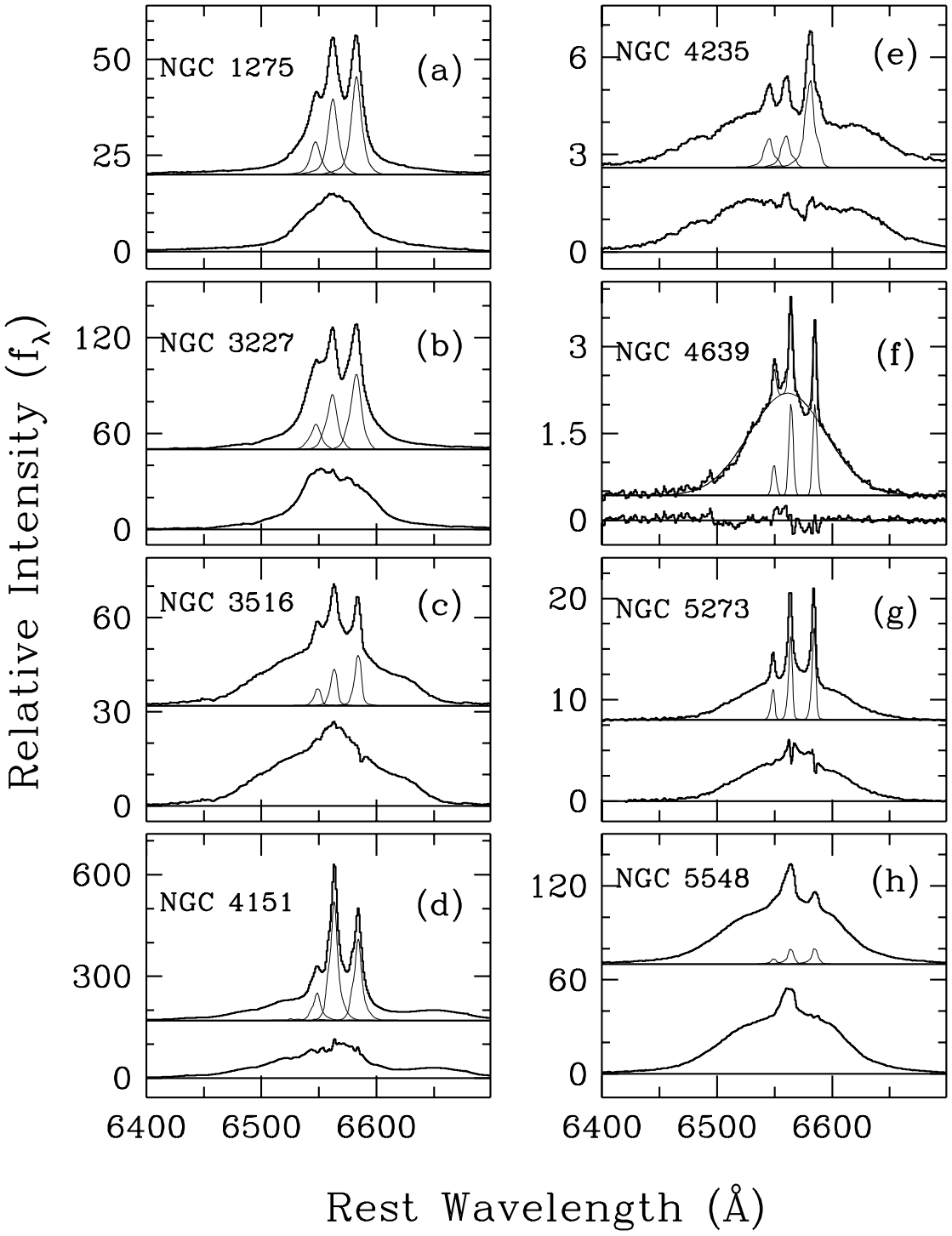


FIG. 6.—Decomposition of the Hα + [N II] region for (*a*) NGC 1275, (*b*) NGC 3227, (*c*) NGC 3516, (*d*) NGC 4151, (*e*) NGC 4235, (*f*) NGC 4639, (*g*) NGC 5273, and (*h*) NGC 5548. Note that, in order to display the full extent of the broader lines of the objects in this figure, the abscissa shows a larger range of wavelengths than in Figs. 7–14.

lines provide a good model for the narrow component of Hα and [N II], then our automatic fitting procedure indeed claims to find a weak ($f_{\rm blend} \approx 13\%$) broad Hα line with FWHM ≈ 2200 km s$^{-1}$ (Fig. 7*a*). Note, however, the sizable residuals near [N II] λ6583, signifying that our adopted model profile does *not* give a very good fit (the model profile is too narrow). Furthermore, although this discrepancy is fairly noticeable in this instance, it could easily have been missed were it not for the high S/N of the spectrum. If we instead assume that the profiles of narrow Hα and [N II] are identical but different from [S II], the algorithm reports an extremely weak broad feature ($f_{\rm blend} \approx 2\%$) shifted toward [N II] λ6583 (Fig. 7*b*: the broad component is not visible at the scale of the plot). For lack of any alternative, the latter set of conditions sometimes must be imposed for objects whose [S II] profile is noticeably different from that of [N II] (e.g., NGC 4321) and in cases for which the [S II] region is simply too noisy (e.g., NGC 266) or corrupted (e.g., NGC 315) to yield a reliable model profile. Finally, if we make no assumptions about the

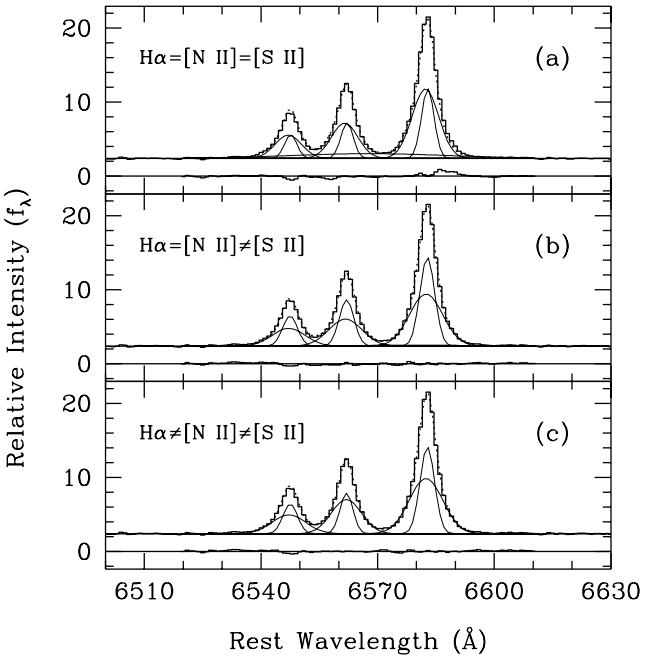


FIG. 7.—Decomposition of the Hα + [N II] region for NGC 1358, assuming that (*a*) the profile of the [S II] lines is identical to the profiles of narrow Hα and [N II], (*b*) the profile of narrow Hα is identical to that of [N II], but these two are different from that of [S II], and (*c*) the profiles of narrow Hα, [N II], and [S II] are independent of each other.

similarity of the narrow Hα, [N II], or [S II] profiles, *no* broad Hα component is required at all (Fig. 7*c*); the final fit finds that the FWHMs of Hα and [N II] (both nearly identical) are only marginally (10%) larger than that of [S II], although their wings are significantly broader (by about 30%). Thus, for NGC 1358 the most conservative conclusion, adopted here, is that broad Hα is not present.

*NGC 1667.*—The narrow-line profiles have extended, non-Gaussian wings that are slightly asymmetric to the red (Fig. 8*a*), giving the false impression that there might be a broad Hα line in this Seyfert 2 nucleus. Both Hα and [N II] have similar profiles, but [S II] is slightly narrower.

*NGC 1961.*—As in NGC 1667, the non-Gaussian (blue) asymmetric wings of the narrow lines mimic broad Hα (Fig. 8*b*). Close inspection of the high-S/N spectrum reveals that the bases of the [S II] lines are somewhat narrower than those of [N II] and Hα, whose profiles are nearly identical. If one had forced all the narrow lines to have the same profile as [S II], one would have concluded incorrectly that broad Hα is present *and* that it is displaced redward of the systemic velocity of the narrow component.

*NGC 2273.*—Each of the narrow lines of the Seyfert 2 nucleus of NGC 2273 (Huchra, Wyatt, & Davis 1982) has faint, extended wings with a blue tail; the lines differ slightly in their profiles. We find no evidence of emission from a BLR (Fig. 8*c*).

*NGC 2342.*—Although the velocity profile of each of the [S II] lines is relatively unblended, it requires two Gaussians for an adequate fit. The resulting model roughly accounts for the Hα + [N II] blend, but significant residuals are seen (Fig. 8*d*). At any rate, broad Hα emission is unlikely to be present.

*NGC 2639.*—Both Keel (1983) and Huchra et al. (1982) recognized that this object emits a broad Hα line. The narrow-line component, however, must be modeled very carefully. A detailed fit to the [S II] lines reveals highly irregular profiles spanning an enormous range of velocities (FWZI $\gtrsim$ 2600 km s$^{-1}$). These mostly account for the apparent strength of the broad Hα line, whose actual contribution is rather modest ($f_{\rm blend} \approx 17\%$, FWHM $\approx$ 3100 km s$^{-1}$: Fig. 8*e*) and very uncertain (estimates differ by at least a factor of 2 among the three fitting methods). Previous profile decomposition of the Hα + [N II] blend, assuming purely Gaussian line shapes (see, e.g., Koratkar et al. 1995), seriously overestimated the broad-line flux.

*NGC 2655.*—The [S II] lines yield an excellent model for the narrow lines, and a broad Hα component is suggested by the decomposition shown in Figure 8*f*. However, the result seems to be highly dependent on the choice of template model used in the starlight subtraction, and we consider the detection to be questionable.

*NGC 2681.*—As for NGC 3031 (Filippenko & Sargent 1988; see also Fig. 1*b*), the two [S II] lines seem to have different widths, although the relatively low S/N of this wavelength region renders the fits somewhat uncertain. Despite the similarity between the profiles of [N II] and [S II] λ6731, the narrow component of Hα has a smaller width than either; this could partly arise from imperfect subtraction of Hα absorption, since an intermediate-age stellar template had to be included in the final starlight model (Paper III). The extended tail redward of [N II] λ6583, apparently absent in [S II], supports the reality of the broad Hα component derived from the profile fitting, but the actual parameters of the broad Hα component are not well constrained (Fig. 8*g*). The extra "bump" near 6523 Å comes from an Fe I feature that is stronger in one of the template galaxies (NGC 205) than in NGC 2681.

*NGC 2768.*—Although the total Hα + [N II] blend hints at the probable presence of weak, broad Hα wings, this suspicion is not confirmed by more detailed line decomposition (Fig. 8*h*). This object is one of the rare cases in which the [S II] lines are actually *broader* than the [N II] lines, although the magnitude of the difference is not great and needs to be evaluated more thoroughly.

*NGC 2787.*—All of the narrow lines can be well modeled by the profile deduced from the [S II] lines. Contrary to the conclusion reached in Paper I, in which the starlight was not yet removed from the spectrum, a fairly prominent ($f_{\rm blend} \approx 35\%$) broad Hα line is present in NGC 2787 (Fig. 9*a*). The extended red wing and apparent offset of the central wavelength of the broad line are most likely artifacts of the depression in the residuals shortward of $\sim$6520 Å. The exact parameters of the broad Hα line in this case are very sensitive to the choice of template, and we have adopted the one shown to achieve the best starlight subtraction over the entire spectrum.

*NGC 2841.*—Despite the somewhat triangular narrow-line profiles, a model from the [S II] doublet fits the complex excellently (Fig. 9*b*), confiming the conclusion of Paper I that broad Hα emission is absent.

*NGC 2911.*—The [S II] lines can fit the Hα + [N II] blend closely but not perfectly, probably because the parameters of the model profile are adversely affected by the somewhat noisy [S II] region. Nevertheless, a broad Hα component can probably be ruled out (Fig. 9*c*).

*NGC 2985.*—A moderately weak ($f_{\rm blend} \approx 22\%$) broad Hα component may be necessary to account for the "shelf" of excess emission discernible in the gaps between Hα and [N II] (Fig. 9*d*). However, because of the low quality of the

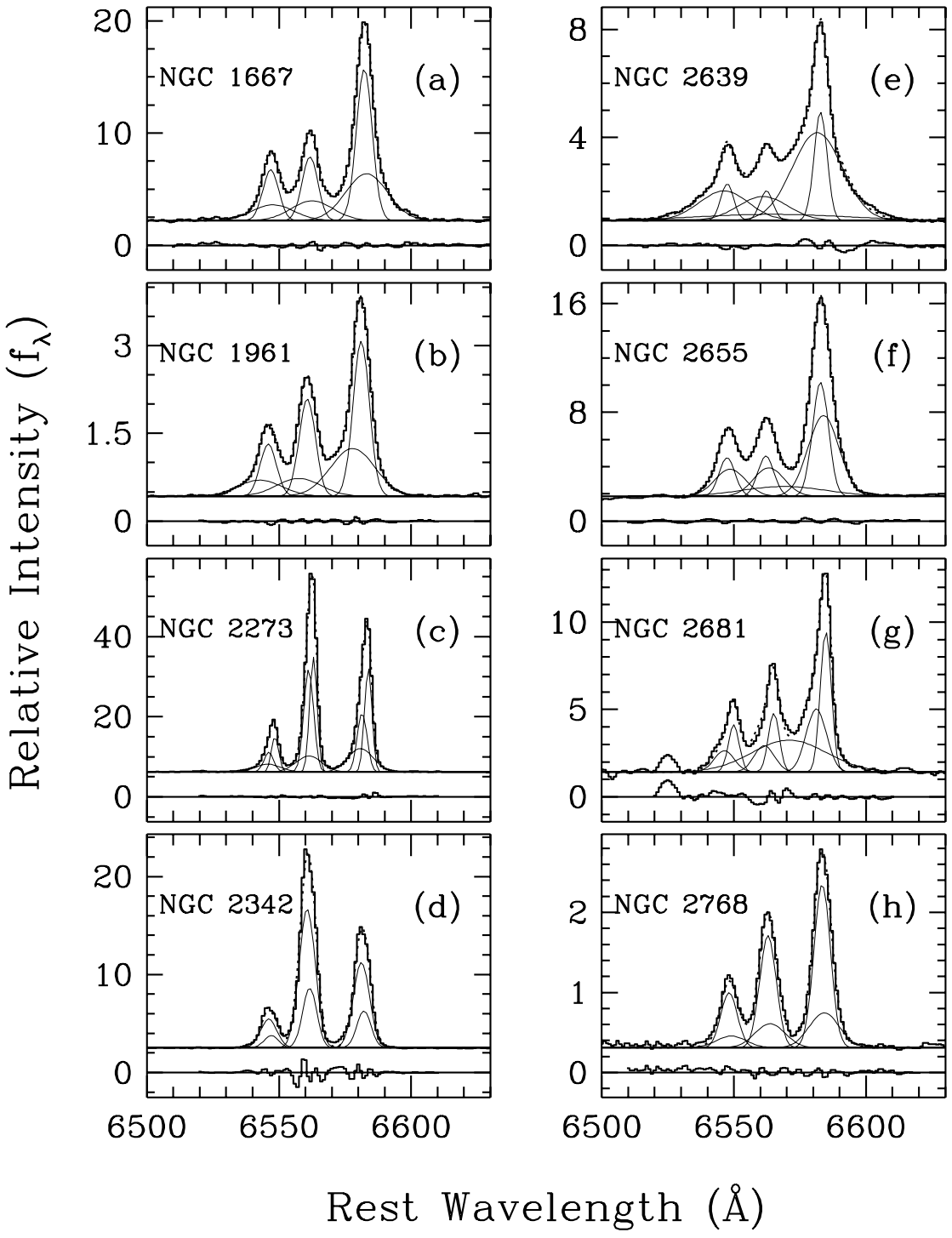


FIG. 8.—Decomposition of the Hα + [N II] region for (*a*) NGC 1667, (*b*) NGC 1961, (*c*) NGC 2273, (*d*) NGC 2342, (*e*) NGC 2639, (*f*) NGC 2655, (*g*) NGC 2681, and (*h*) NGC 2768.

data in the [S II] region, we cannot rule out the possibility that the excess emission originates from weak, intrinsically broad wings in the narrow-line profile. Thus, at this point, we will regard the broad Hα detection only as tentative. That the narrow component of Hα is slightly narrower than [N II] (resulting in relatively pronounced residuals) can probably be attributed to imperfect removal of Hα absorption.

*NGC 3031.*—As was first discovered by Peimbert & Torres-Peimbert (1981), confirmed by Shuder & Osterbrock (1981), and subsequently studied in greater detail by Filippenko & Sargent (1988), NGC 3031 (M81) has a conspicuous ($f_{\rm blend} \approx 57\%$) broad Hα line with FWHM ≈ 2650 km $s^{-1}$. The recent detections of nonthermal X-ray emission (Petre et al. 1993; Ishisaki et al. 1996), a highly compact VLBI radio core (Bietenholz et al. 1996), and a nonstellar, featureless ultraviolet continuum (Ho et al. 1996) have made NGC 3031 the first LINER whose multiwavelength spectrum has been studied in depth. The narrow-line spectrum is characterized by a large range of line widths because of

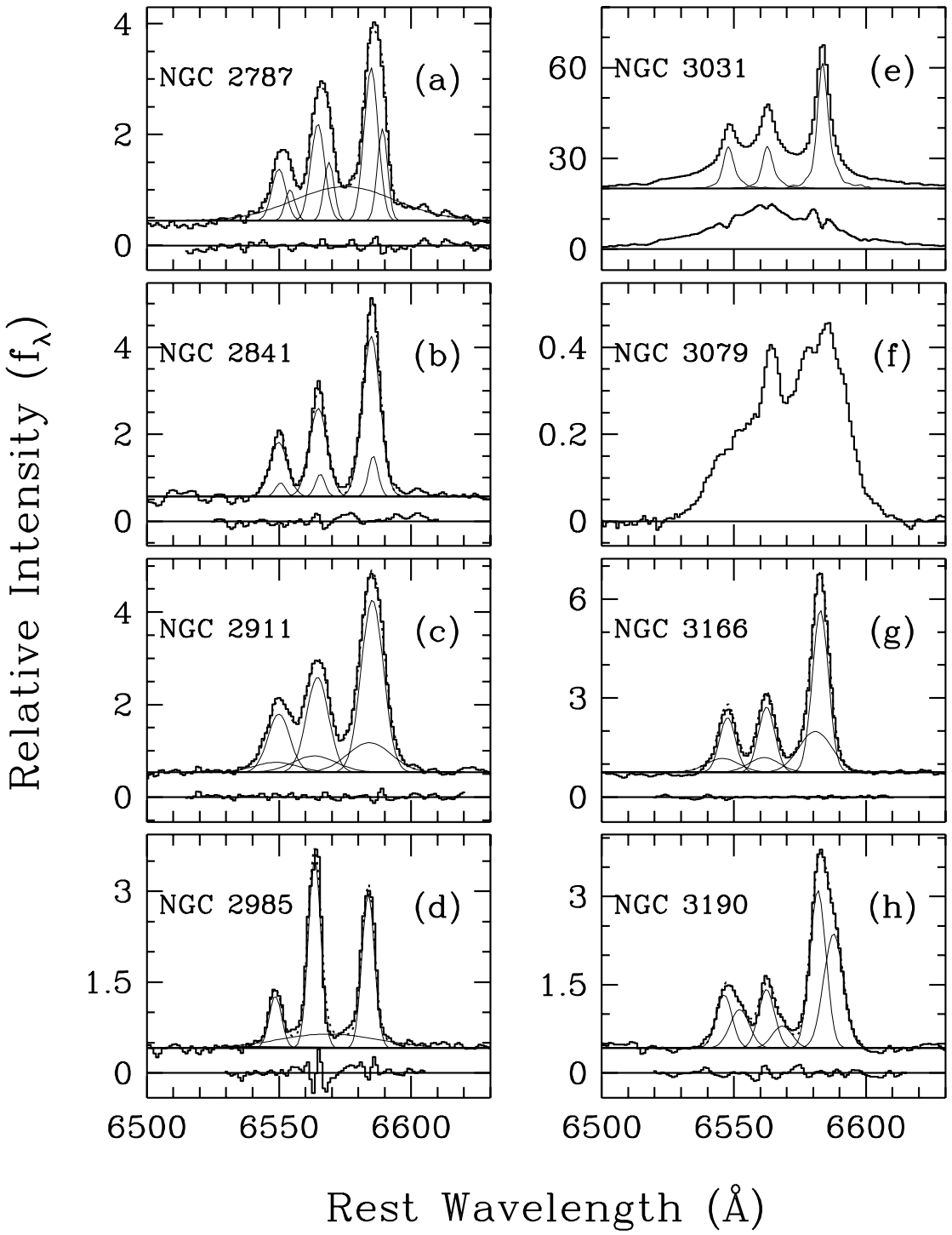


FIG. 9.—Decomposition of the Hα + [N II] region for (*a*) NGC 2787, (*b*) NGC 2841, (*c*) NGC 2911, (*d*) NGC 2985, (*e*) NGC 3031, (*f*) NGC 3079, (*g*) NGC 3166, and (*h*) NGC 3190.

density stratification (Filippenko & Sargent 1988; Ho et al. 1996). Although a model of [S II] λ6731 roughly matches [N II] and narrow Hα (see, e.g., Filippenko & Sargent 1988 and Fig. 9*e*), it is obvious from the residuals that the base of [N II] is somewhat wider than that of [S II]. Moreover, the two [S II] lines clearly have different widths (Filippenko & Sargent 1988; Fig. 1*b*). The dominance of the broad Hα component makes it difficult to derive the true profile parameters of [N II]. Both Hβ and Hγ have broad components (see also Filippenko & Sargent 1988), and spectra taken with the *Hubble Space Telescope* (*HST*) show several additional broad lines in the ultraviolet (Ho et al. 1996).

*NGC 3079.*—The large strengths of [O II] λ3727 (Heckman, Balick, & Crane 1980) and [O I] λ6300 (Paper III) relative to [O III] λ5007 in the nucleus of NGC 3079 qualify it as a LINER according to the definition of Heckman (1980). Adhering to the convention of Paper III, on the other hand, the [O III]/Hβ ratio puts the nucleus in the category of Seyfert galaxies; however, it should be noted that the Hβ line is very weak and uncertain and that the

excitation could be lower. As described extensively by Filippenko & Sargent (1992) and Veilleux et al. (1994) and is clearly illustrated in Figure 9*f*, the kinematics of the line-emitting gas near the nucleus of this edge-on SBc galaxy are extremely complicated. The central starburst appears to dominate the energetics, although some contribution from an AGN cannot be excluded (Veilleux et al. 1994). In view of the complexity of the velocity field of the gas, it is not surprising that we were unsuccessful in achieving a satisfactory decomposition of the Hα + [N II] blend. (We do not show any of the trial fits in Fig. 9*f*.) Within our 2″ × 4″ extraction aperture, the [S II] line profile does not entirely match the shape of the [N II] lines, and Hα seems to have a narrow core (Fig. 9*f*), perhaps because of superposed emission from H II regions, which is absent from [N II] and [S II]. Judging by the spatial variation of the emission-line spectrum (Veilleux et al. 1994), these profile differences most likely reflect variations in excitation or physical conditions among the discrete gas elements included in our integrated spectrum. Without adequate constraints on the intrinsic narrow-line profiles, it is virtually impossible to fit the broad Hα component with confidence. Thus, although Stauffer (1982) and Keel (1983) suspected that broad Hα was present in this object, we agree with Filippenko & Sargent (1992) that it is premature to come to any firm conclusions.

*NGC 3166*.—As with NGC 1358, the imperfect match between the [S II] model and the [N II] lines can deceptively mimic a low-contrast, apparently redshifted, broad Hα feature. We will opt for the more conservative viewpoint that such a feature is spurious and simply fit each of the narrow lines with two Gaussians (Fig. 9*g*).

*NGC 3190*.—The narrow lines are unusually broad (FWHM ≈ 500 km s$^{-1}$) and have a clear red asymmetry, but there is no evidence for a broad component of Hα (Fig. 9*h*). The Hα line has a noticeably smaller width than [N II], most likely resulting from imperfect starlight subtraction.

*NGC 3226*.—Despite a fairly noisy spectrum, the tail redward of [N II] λ6583 is also present in [S II] λ6731. A total of three Gaussians was used to model the unusual narrow-line profile, and we succeeded in extracting a moderately strong broad Hα component from the complicated blend (Fig. 10*a*).

*NGC 3227*.—In order to quantitatively measure the extremely broad (FWZI ≈ 16,000 km s$^{-1}$) Hα line of this well-known Seyfert 1 nucleus, we carefully removed the narrow-line contribution of the blend by scaling an accurate model constructed from [S II] (Fig. 6*b*). It is difficult to tell whether all the narrow lines have the same profile, but this is not crucial for the purposes of measuring such a strong, broad Hα line. Broad Hβ and Hγ are both very prominent. The broad lines in this object are known to be variable (see, e.g., Winge et al. 1995); the spectrum shown here was taken on 1986 March 29 UT.

*NGC 3245*.—Along with NGC 5005, the line profiles of this galaxy exhibit one of the most complicated velocity structures in this survey (Fig. 10*b*). The rotation curve rises very steeply within the central 4″ in the two-dimensional spectrum, causing each line to have a double-horned profile. Despite this complexity, each line can be well modeled by a combination of three Gaussian components: one for the nucleus and one each for the receding and approaching sides of the disk. While the same combination of components fits [N II] and [S II], the central (nuclear) component of Hα is weaker than the two disk components, as is obvious from the "dip" in the center of the profile. This is simply a manifestation of the higher [N II]/Hα and [S II]/Hα ratios for the LINER component centered on the nucleus (classified in Paper III as a transition object). A very faint ($f_{\rm blend} \approx 12\%$), broad (FWHM ≈ 2650 km s$^{-1}$) component of Hα is suggested by our decomposition, but the result, unfortunately, is ambiguous, because it seems to depend on the choice of template model used in the starlight subtraction.

*NGC 3367*.—This is an Sc galaxy with a prominent nucleus showing emission features of Wolf-Rayet stars (Paper II). The narrow lines have distinctly non-Gaussian profiles with obvious blue asymmetry (Fig. 10*c*). The relatively wide bases of the narrow lines give the impression that there might be broad Hα, but this is not confirmed by detailed modeling, which shows that the [S II] lines have the same profiles.

*NGC 3516*.—We determined the narrow-line spectrum of this well-known Seyfert 1 nucleus (Boksenberg & Netzer 1977) quite accurately, using a model derived from [S II] (Fig. 6*c*). The resulting fits give ([N II] λ6583)/Hα = 1.3, ([S II] λλ6716, 6731)/Hα = 0.70, and ([O I] λ6300)/Hα = 0.15. The broad-line component is also clearly present in Hβ and Hγ.

*NGC 3642*.—Broad Hα emission is easily discernible (Paper I) because of the small widths of the narrow lines (Fig. 10*d*). As with many other objects, however, the broad-line component would be overestimated if the narrow lines were modeled as single Gaussians, since the bases of the narrow lines have extended wings. A reliable two-Gaussian model for [N II] was derived from [S II]; the narrow component of Hα evidently has a larger core-to-base ratio (and hence smaller FWHM) than [N II]. Since the stellar population of the nucleus of NGC 3642 does not appear to have exceptionally strong Balmer absorption, the difference in profile between Hα and [N II] probably does not come from undersubtraction of Hα absorption; instead, the most likely explanation is that the narrow-line spectrum is partly contaminated by emission from circumnuclear H II regions, whose [N II]/Hα ratios are smaller than those of AGNs.

*NGC 3718*.—As noted in Paper I, broad Hα emission is definitely present. Constraining the narrow lines with a [S II] model, we find that a broad component with FWHM = 2350 km s$^{-1}$ accounts for ∼50% of the total flux of the blend. The centroid of the broad component of Hα is redshifted by 430 km s$^{-1}$ with respect to the narrow component (Fig. 10*e*). One possible interpretation of the velocity redshift seen in the broad Hα line in NGC 3718 is that the emission is scattered off of outflowing electrons in the narrow-line region, as in the well-known case of NGC 1068 (Antonucci & Miller 1985; Miller et al. 1991). It should be remembered, however, that systematic errors in the determination of the continuum level or in our assumptions about the profiles of the narrow lines can also possibly lead to apparent velocity shifts (see notes on NGC 266, 1358, 1961, and 3166).

*NGC 3884*.—The extended tail of faint emission redward of [N II] λ6583 betrays a hidden broad-line component in NGC 3884 (Keel 1983; Paper I; Fig. 10*f*). Unfortunately, the high recession velocity of the object shifted part of the [S II] λ6731 line out of our spectral range. The narrow-line model profile, derived solely from [S II] λ6716, is therefore not well constrained. In particular, we could not verify

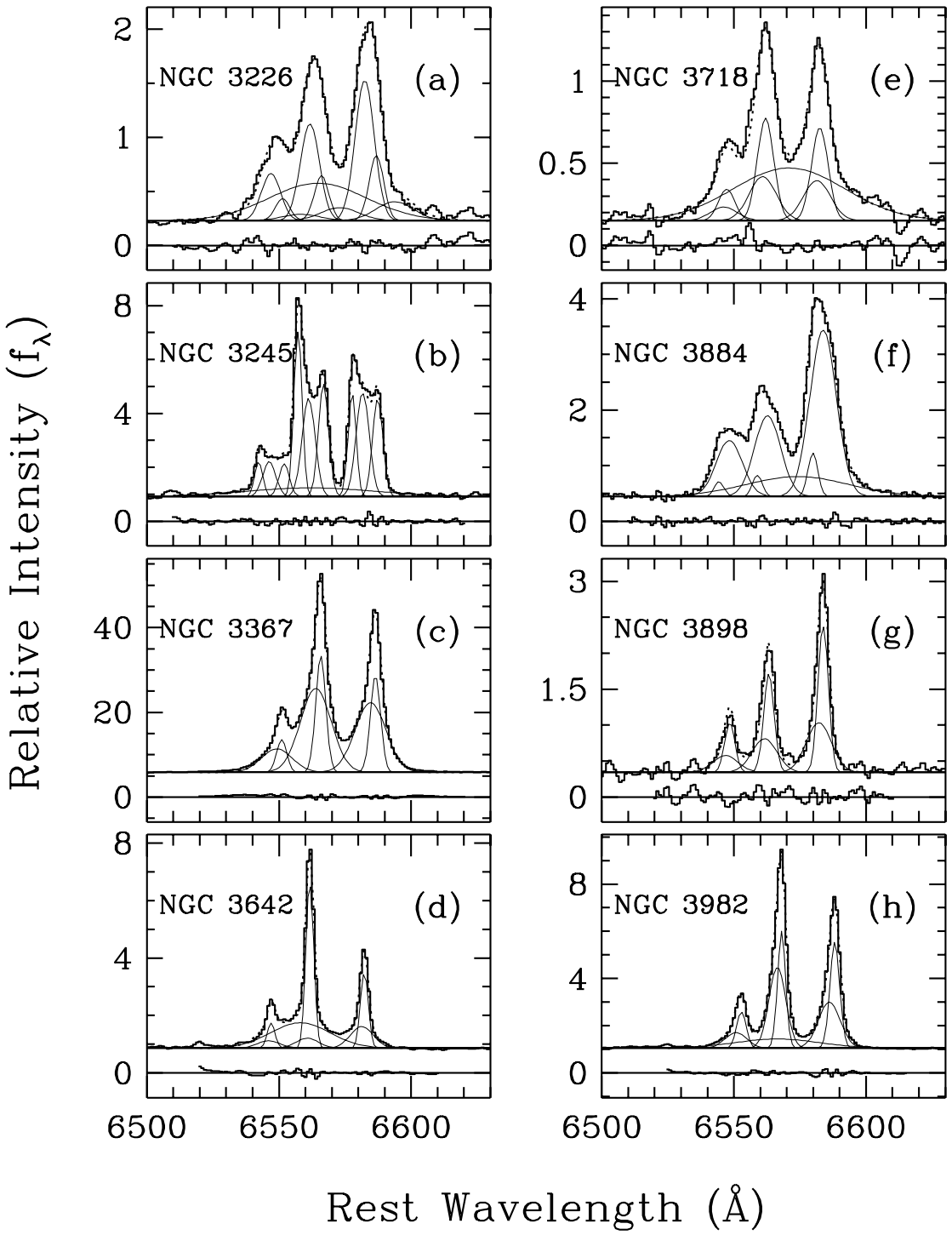


FIG. 10.—Decomposition of the Hα + [N II] region for (*a*) NGC 3226, (*b*) NGC 3245, (*c*) NGC 3367, (*d*) NGC 3642, (*e*) NGC 3718, (*f*) NGC 3884, (*g*) NGC 3898, and (*h*) NGC 3982.

whether the extended tail of emission is truly absent from the [S II] lines. Nevertheless, neither [O I] nor [O III] shows any obvious signs of such extreme red asymmetry in their profiles, leading us to conclude that the deduced broad Hα component is very likely to be real.

*NGC 3898.*—The profiles of the [S II] lines do not match those of narrow Hα and [N II] in detail. This, coupled with the fact that the spectrum does not have very high S/N, leads to ambiguity regarding the detection of broad Hα (Fig. 10*g*). We will adopt the more conservative assumption that broad Hα is not present; it would be highly desirable to verify this with data of higher S/N.

*NGC 3982.*—This Seyfert 2 nucleus (Paper III) contains an extremely faint ($f_{\rm blend} \approx 12\%$), broad Hα component (Fig. 10*h*). Although the broad Hα is apparent only after detailed profile fitting, we are reasonably confident of this detection. [N II] has the same profile as [S II], but narrow Hα differs slightly.

*NGC 3998.*—Broad Hα is unmistakably present in this famous LINER (Fig. 11*a*). as was already known from

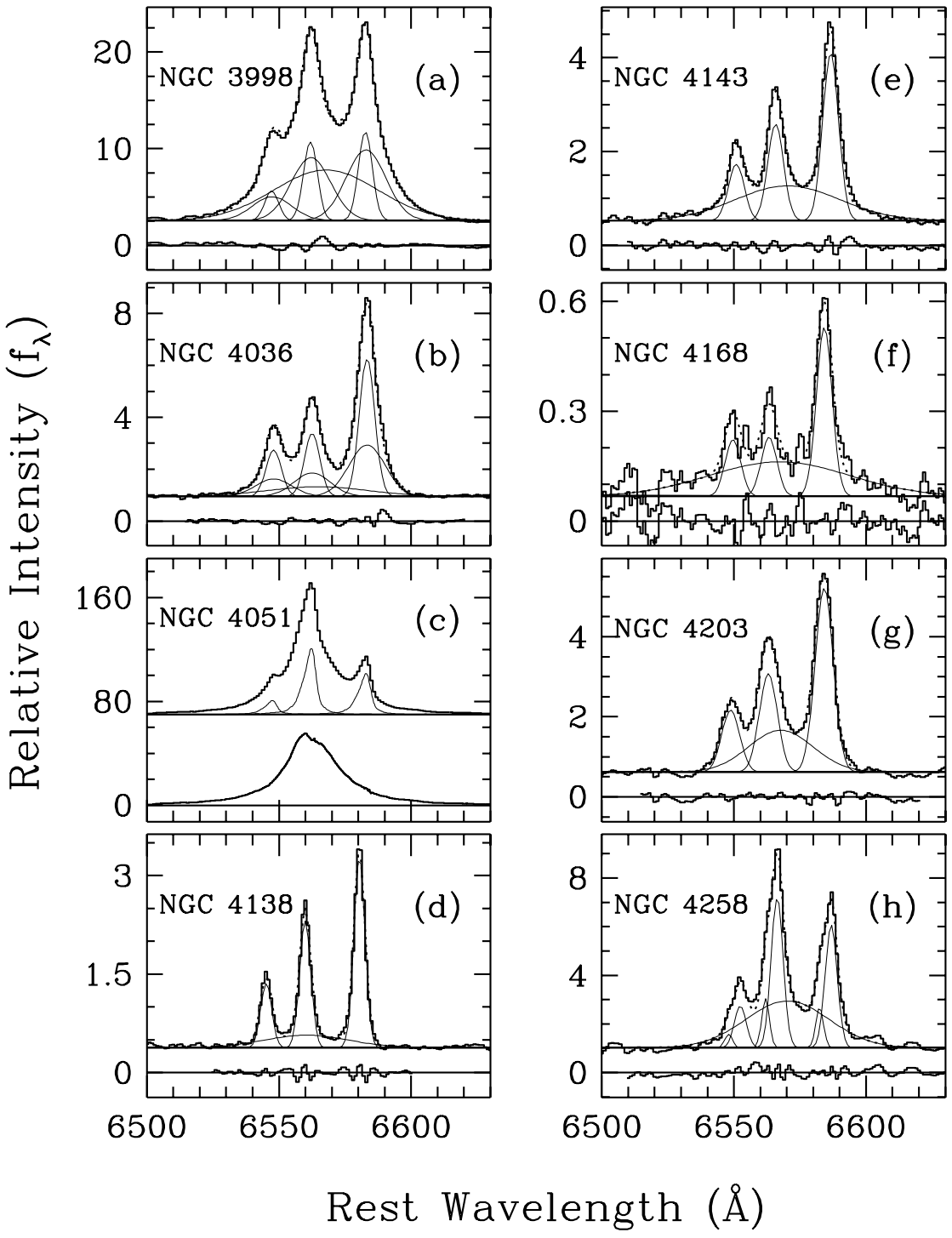


FIG. 11.—Decomposition of the Hα + [N II] region for (*a*) NGC 3998, (*b*) NGC 4036, (*c*) NGC 4051, (*d*) NGC 4138, (*e*) NGC 4143, (*f*) NGC 4168, (*g*) NGC 4203, and (*h*) NGC 4258.

several previous studies (Heckman 1980; Blackman, Wilson, & Ward 1983; Keel 1983; Paper I). Reichert et al. (1992) found that Mg II λ2800 also has a broad component, similar in width to broad Hα. The narrow-line profile, as judged from the [S II] doublet, is quite systematic and can be represented by the sum of a narrow and a broader Gaussian. The flux of broad Hα, as determined from our three standard fitting methods, showed excellent agreement (differing by less than 5% from each other), and we obtained the final value by averaging all three results. The adopted broad Hα component contains ∼37% of the flux of the entire Hα + [N II] blend and has widths of FWHM ≈ 2150 km s$^{-1}$ and FWZI ≳ 5000 km s$^{-1}$. Broad Hβ is also present.

*NGC 4036.*—A broad component of Hα seems necessary to adequately model the Hα + [N II] complex (Fig. 11*b*), though the broad Hα line is faint ($f_{\rm blend} \approx 14\%$), confirming the preliminary analysis of Paper I. The narrow-line profile from [S II] has extended, non-Gaussian wings but is very symmetric.

*NGC 4051*.—With an absolute blue magnitude of only $-15.6$ (Véron 1979, assuming $H_0 = 50$ km s$^{-1}$ Mpc$^{-1}$), the nucleus of NGC 4051 can be considered the least luminous "classical" type 1 Seyfert (Weedman 1976). As with other prominent Seyfert 1 nuclei (e.g., NGC 3516; Fig. 6*c*), we removed the narrow-line contribution to the complex with a model constructed from the [S II] lines (Fig. 11*c*). The broad H$\alpha$ line has unusually small widths (FWHM $\approx$ 1000 km s$^{-1}$, FWZI $\approx$ 5900 km s$^{-1}$) compared with other objects of its class (e.g., NGC 4151, NGC 5548), and this object most likely belongs to the group of "narrow-lined" Seyfert 1 nuclei (Osterbrock & Pogge 1985). Both H$\beta$ and H$\gamma$ also have broad components.

*NGC 4138*.—This is one of several previously unrecognized Seyfert galaxies discovered in our survey (Paper III). The narrow lines of H$\alpha$, [N II], and [S II] have symmetric profiles that can be well described by single Gaussians. Visual inspection of the regions between H$\alpha$ and [N II], further confirmed by detailed fitting, reveals a relatively weak broad H$\alpha$ line responsible for $\sim$23% of the emission from the entire blend (Fig. 11*d*).

*NGC 4143*.—As the bases of the [S II] lines are not significantly wider than that of a single Gaussian, the extended wings of the H$\alpha$ + [N II] complex probably signify the presence of a prominent broad H$\alpha$ component. Indeed, a four-component Gaussian fit to the complex yields a broad line (FWHM $\approx$ 2100 km s$^{-1}$) containing a large fraction ($f_{\rm blend} \approx 45\%$) of the emission (Fig. 11*e*). Broad H$\beta$ may also be present.

*NGC 4151*.—The highly variable broad-line emission of this famous Seyfert 1 nucleus has been the target of intensive spectroscopic monitoring (see, e.g., Maoz et al. 1991; Kaspi et al. 1996). We modeled the asymmetric narrow-line profile of [S II] with a combination of three Gaussians, which were then scaled and subtracted to remove the narrow lines from the complex (Fig. 6*d*). The broad H$\alpha$ profile of the spectrum shown (taken on 1986 March 19 UT) exhibits a prominent blue asymmetry; the extra hump near 6600 Å partially comes from broad He I $\lambda$6678 emission. Broad H$\beta$ and H$\gamma$ are present in the blue spectrum, as is He II $\lambda$4686.

*NGC 4168*.—Because of the small equivalent widths of the emission lines in this elliptical galaxy, the S/N of the starlight-subtracted spectrum is rather low, and its classification is subject to considerable uncertainty. Taken at face value, the intensity ratios of the emission lines qualify NGC 4168 as a Seyfert galaxy (Paper III). Despite the noise in the spectrum and the large uncertainties associated with the final parameters of the fit, a rather obvious broad H$\alpha$ feature is apparent even in the unfitted data (Fig. 11*f*).

*NGC 4203*.—Broad H$\alpha$ is detected unambiguously in this LINER (Fig. 11*g*). The fairly symmetric narrow lines of H$\alpha$, [N II], and [S II] can be fitted by a single Gaussian with FWHM $\approx$ 350 km s$^{-1}$.

*NGC 4235*.—The broad H$\alpha$ profile of this Seyfert 1 nucleus (Abell, Eastmond, & Jenner 1978) has a peculiar secondary hump redward of [N II] $\lambda$6583, resembling that of NGC 7213 (Filippenko & Halpern 1984). The narrow-line profile, as judged by modeling [S II], requires a superposition of three Gaussians to reproduce its irregular shape (Fig. 6*e*). The profile of [N II] $\lambda$6583 appears to have additional structure not present in [S II], but, for the present purposes, we neglect this subtlety. A very prominent broad component is visible at H$\beta$.

*NGC 4258*.—With [O III] $\lambda$5007/H$\beta \approx 10$, NGC 4258 (M106) harbors a Seyfert nucleus (Paper III), not a LINER (see, e.g., Heckman 1980; Greenhill et al. 1995). VLBI observations recently have furnished dynamical evidence that the nucleus has an extremely high mass density, probably indicative of a supermassive black hole (Miyoshi et al. 1995; Greenhill et al. 1995). A broad H$\alpha$ component is apparent in the high-resolution nuclear spectra published by Stüwe, Schulz, & Hühnermann (1992; see their Fig. 2), although the detailed shape of the H$\alpha$ + [N II] complex is somewhat different from ours (Fig. 11*h*) because these authors did not correct their data for starlight contamination. Stüwe et al. questioned the reality of the broad H$\alpha$ line, arguing that Lorentzian profiles alone, instead of Gaussians, can give an acceptable fit to the complex without invoking an extra broad component. But, as we have shown throughout this paper, any single analytic profile, whatever its form, generally gives a poor representation of the intrinsic shapes of the narrow lines, and a more involved procedure must be applied. Using a model for the narrow lines derived from the [S II] profile, a very pronounced broad H$\alpha$ component, as was previously noticed by Stauffer (1982) and Paper I, is inferred from our fit (Fig. 11*h*). The narrow lines have an obvious blue asymmetry and have FWHMs of about 290 km s$^{-1}$. The broad H$\alpha$ component can be represented reasonably well by a Gaussian of FWHM $\approx$ 1700 km s$^{-1}$, from which we deduce a luminosity (not corrected for extinction) of $4.5 \times 10^{38}$ ergs s$^{-1}$ (assuming a distance of 6.8 Mpc; Tully 1988). Note that Wilkes et al. (1996) found that the polarized spectrum of the nucleus exhibits emission lines that are broader than those in the unpolarized spectrum. The "broad" lines in this case, however, only have FWHM $\approx$ 1000 km s$^{-1}$ and are seen both in the permitted lines and in the forbidden lines. This component, therefore, is different from the broad component we observe associated with H$\alpha$, which we attribute to the classical BLR. A weak broad H$\alpha$ component may be present in the polarized spectrum of Wilkes et al., but the S/N of their data does not permit a clear determination.

*NGC 4261*.—Images from *HST* reveal an extended disk surrounding the LINER nucleus of NGC 4261 (Jaffe et al. 1993), and dynamical analysis suggests the presence of a supermassive black hole (Jaffe et al. 1996; Ferrarese, Ford, & Jaffe 1996). The [S II] lines in our data are not of sufficiently high quality to yield a reliable model for the narrow lines. Nevertheless, all the narrow lines look quite symmetric and have broad wings. We represented each line with a combination of two Gaussians centered at the same wavelength (Fig. 12*a*). In most of the lines (H$\gamma$, H$\beta$, [N II], H$\alpha$, and [S II]), the narrow core has FWHM $\approx$ 300 km s$^{-1}$, and the broader base has FWHM $\approx$ 900 km s$^{-1}$. Some of the forbidden lines with higher critical densities, however, also have larger line widths. [O III] $\lambda\lambda$4959, 5007 has a core with FWHM $\approx$ 300 km s$^{-1}$ but a base with FWHM $\approx$ 1500 km s$^{-1}$, while [O I] $\lambda$6300 is best modeled with two Gaussians of FWHM $\approx$ 650 km s$^{-1}$ and 1400 km s$^{-1}$. Jaffe et al. (1996) recently performed a detailed analysis of the optical emission-line profiles of the nucleus of NGC 4261 based on ground-based spectra. Their results are consistent with ours, the most noticeable difference being that they detected much broader lines than we did. The [N II], H$\alpha$ and [S II] lines in the Jaffe et al. spectrum, for instance, have cores with FWHM $\approx$ 410–490 km s$^{-1}$ and wings with FWHM $\approx$ 2700–3500 km s$^{-1}$. We attribute this difference

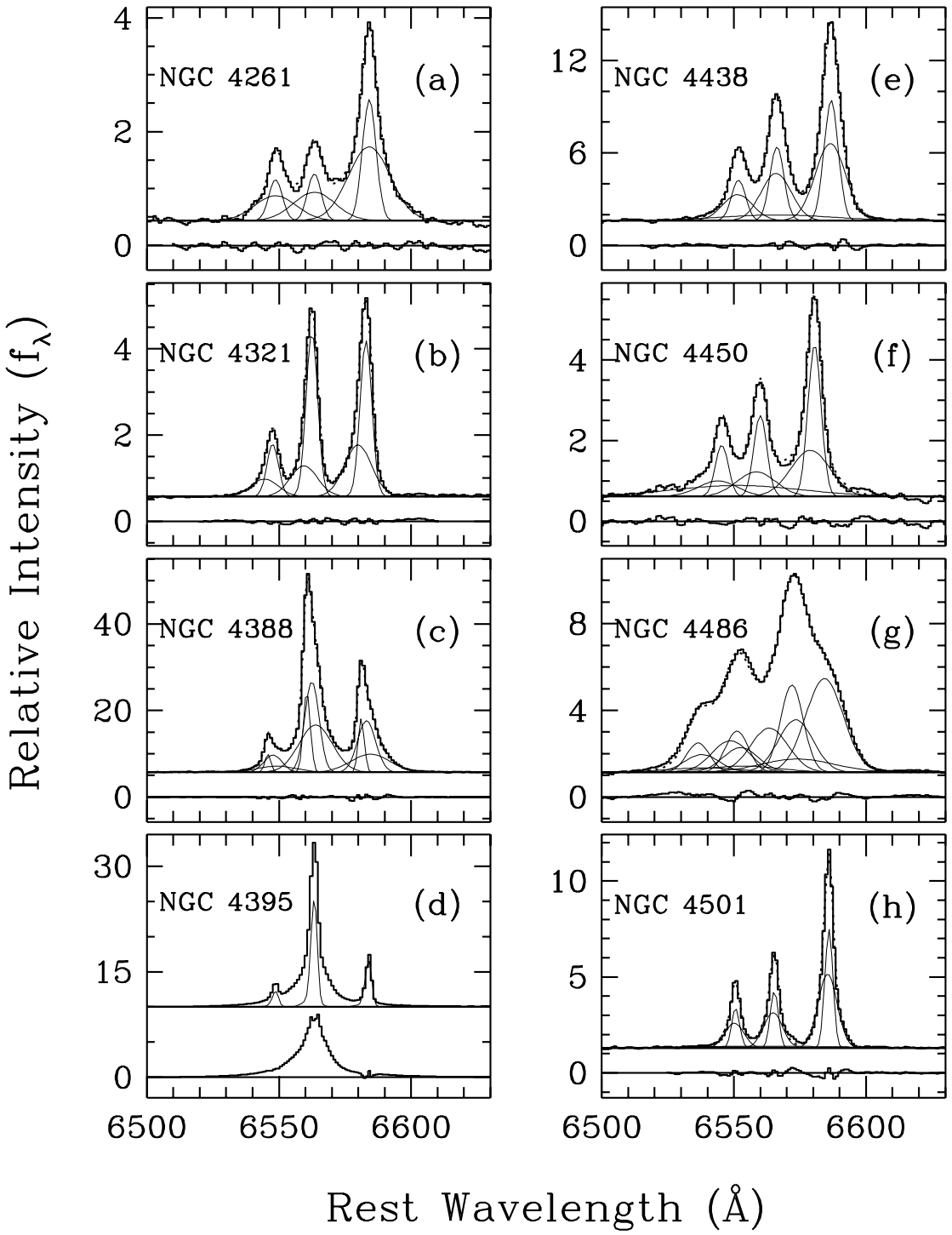


FIG. 12.—Decomposition of the Hα + [N II] region for (*a*) NGC 4261, (*b*) NGC 4321, (*c*) NGC 4388, (*d*) NGC 4395, (*e*) NGC 4438, (*f*) NGC 4450, (*g*) NGC 4486, and (*h*) NGC 4501.

to the fact that Jaffe et al. acquired their data using a narrower slit than we did (1.″1 vs. 2″) and under conditions of better seeing (1″ vs. 1.″5). Because the widths of the emission lines in NGC 4261 increase very rapidly close to the nucleus (Ferrarese et al. 1996), the better spatial resolution of the Jaffe et al. spectrum naturally samples gas with higher velocities. Consistent with Jaffe et al., we find no Hα emission arising from a BLR. The small-aperture (0.″1) *HST* spectra of Ferrarese et al. (1996) also show no obvious signs of broad Hα.

*NGC 4278.*—As illustrated in Figure 2, a relatively weak, broad Hα line can be extracted from NGC 4278, an elliptical radio galaxy with a LINER nucleus. Rotational broadening contributes to the large width (FWHM = 480 km $s^{-1}$) of the narrow lines, each of which is well modeled by the sum of two Gaussians.

*NGC 4321.*—The extended and highly asymmetric wings of the narrow lines in the transition nucleus of NGC 4321 (M100) superficially resemble broad Hα emission. Indeed, if one naively assumed that the [S II] lines can be used to

model the narrow components of Hα and [N II], one could force a broad feature in the fit (e.g., as in NGC 1358). Fortunately, the data have high enough S/N that differences in the narrow-line profiles are discernible. An excellent fit to the complex can be achieved simply by constraining narrow Hα and [N II] to have identical profiles (Fig. 12*b*), and no broad Hα is necessary to fit this spectrum.

*NGC 4388.*—Originally classified as a Seyfert 2 galaxy (Phillips & Malin 1982), the nucleus of NGC 4388 in fact contains very faint wings of broad Hα emission (Stauffer 1982; Paper I) with FWZI $\approx$ 6000 km s$^{-1}$ (Shields & Filippenko 1988, 1996). In addition, Shields & Filippenko discovered broad Hα emission in at least two off-nuclear positions, which they interpreted as scattered radiation from a largely hidden Seyfert 1 nucleus similar to that seen in NGC 1068 (Miller et al. 1991). As in most nuclei discussed in this study, the narrow lines themselves have extended, asymmetric wings; these have to be properly removed to accurately measure the broad Hα flux (Fig. 12*c*)' Using a model profile derived from [S II], each narrow line is well represented by a combination of three Gaussians. The resulting broad line (FWHM $\approx$ 3900 km s$^{-1}$) contains a mere 2% $\pm$ 2% of the flux of the entire blend. Because of the scale of the plot, the broad line is barely visible in Figure 12, but Figure 14 of Paper I more clearly illustrates its presence.

*NGC 4395.*—This galaxy holds the special distinction of hosting the least luminous ($M_B = -9.8$ mag) and nearest (2.6 Mpc) Seyfert 1 nucleus known (Filippenko & Sargent 1989). As in Filippenko & Sargent, the narrow components of Hα and [N II] were removed from the blend, using [S II] as a model (Fig. 12*d*). The narrow lines, whose FWHMs are 40–50 km s$^{-1}$ (Filippenko & Ho 1997), are unresolved at the current resolution. As confirmed by the high-resolution spectra of Filippenko & Ho, the narrow-line profiles all have a blue asymmetric tail. Although the FWHM of the broad Hα component is only $\sim$500 km s$^{-1}$, the base of the line stretches to a FWZI of $\sim$5000 km s$^{-1}$ (less than the 7000 km s$^{-1}$ quoted by Filippenko & Sargent 1989). A broad component is present in a number of other optical (Filippenko & Sargent 1989) and ultraviolet (Filippenko, Ho, & Sargent 1993) emission lines.

*NGC 4438.*—With a strength of only 9% of the total Hα + [N II] blend, the broad Hα component in NGC 4438 is among the weakest of our probable detections. The high S/N of the starlight-subtracted spectrum allowed us to construct an accurate profile model from [S II] that matched well the profiles of the other narrow lines. Very faint residual wings were evident on both sides of [N II] even after the narrow lines were removed, and the best fit was achieved with the addition of a broad Gaussian with FWHM $\approx$ 2050 km s$^{-1}$ (Fig. 12*e*).

*NGC 4450.*—The narrow-line profiles of this LINER show extended, slightly asymmetric wings that largely contribute to the broad base of the complex (Fig. 12*f*). However, additional low-level emission extends beyond the wings of [N II], and a full analysis of the blend indicates the probable presence of a fairly weak ($f_{\rm blend} \approx 20\%$; FWHM $\approx$ 2300 km s$^{-1}$) broad Hα line, confirming the suggestions of Stauffer (1982) and Paper I.

*NGC 4486.*—Although the presence of weak extensions on either side of the [N II] lines led us to suspect, in Paper I, that broad Hα might exist in the nucleus of this famous active galaxy (M87), careful inspection of the spectrum after starlight subtraction indicates that the [S II] lines may have similar wings in their profiles. Note also that the nuclear spectrum obtained with *HST* using a 0.″26 aperture (Harms et al. 1995) shows that [N II] and [S II] have similar profiles. The enormous widths of the emission lines (FWHM $\approx$ 1000–1100 km s$^{-1}$), unfortunately, cause severe blending, and so no unique model can be determined for the highly asymmetric [S II] lines based on our data. With the assumption that both [S II] lines have the same profile, each line can be modeled by a combination of four Gaussian components. If we apply this model to all three lines in the Hα + [N II] blend, it can be seen that the fit is rather poor (Fig. 12*g*). Adding an additional broad Gaussian to the fit will obviously reduce the residuals, and such a component can be interpreted as broad Hα emission, but we choose not to do so because of the above ambiguities. The small-aperture spectrum of Harms et al. also does not show broad emission associated with Hα, apart from the extended wings seen in all the narrow lines.

*NGC 4501.*—NGC 4501 harbors a previously unrecognized Seyfert 2 nucleus (Paper III). Judging by the faint wings on either side of [N II], it appears that an extremely faint ($f_{\rm blend} \approx 9\%$), broad (FWZI $\approx$ 5000 km s$^{-1}$) Hα component is present (Fig. 12*h*), but its detailed parameters are uncertain because of ambiguities in the true shape of the narrow lines.

*NGC 4565.*—The large [O III]/Hβ ($\sim$9) and [N II]/Hα ($\sim$2.5) ratios qualify NGC 4565 as a Seyfert galaxy. A relatively faint ($f_{\rm blend} \approx 16\%$) broad Hα component is seen in the Hα + [N II] blend after fitting the narrow lines with a model of [S II] λ6731 (Fig. 13*a*). If this detection is correct, the broad Hα luminosity ($8 \times 10^{37}$ ergs s$^{-1}$) is the lowest yet found in any active nucleus, even smaller than that of NGC 4395. As in the case of NGC 3031 (Fig. 1*b*), [S II] λ6716 is narrower than [S II] λ6731.

*NGC 4579.*—Broad Hα emission has long been known to be present in this LINER/Seyfert nucleus (Stauffer 1982; Keel 1983; Paper I), but its strength is substantially weaker than that deduced from decomposition of the narrow lines using single Gaussians. The extended, asymmetric base of [S II] largely accounts for most of the broad base of the Hα + [N II] complex. Nevertheless, a detailed multicomponent fit undeniably requires a moderately strong ($f_{\rm blend} \approx 21\%$) broad Hα line (Fig. 13*b*). The BLR in NGC 4579 recently has also been revealed in the ultraviolet (Barth et al. 1996).

*NGC 4594.*—Contrary to the conclusion in Paper I, we find no evidence of broad Hα in the LINER nucleus of NGC 4594 (also known as the Sombrero galaxy and as M104). Careful inspection of the line profiles indicates that the [S II] lines have large widths (FWHM $\approx$ 500 km s$^{-1}$) and extended wings (FWZI $\approx$ 3000 km s$^{-1}$); in fact, this is one of the rare instances in which the [S II] lines are actually broader than the narrow Hα and [N II] lines. The blend was modeled assuming that Hα and [N II] have identical profiles, each of which can be represented by the sum of two Gaussians (Fig. 13*c*). Note that broad Hα *has* been detected in the recent, small-aperture *HST* spectra of Kormendy et al. (1997), illustrating the advantages that can be gained from data of high spatial resolution.

*NGC 4636.*—A moderately strong broad Hα component is apparent in the starlight-subtracted spectrum (Fig. 13*d*). Although the [S II] region is too noisy to provide a reliable model for the narrow lines, the narrow Hα and [N II] lines

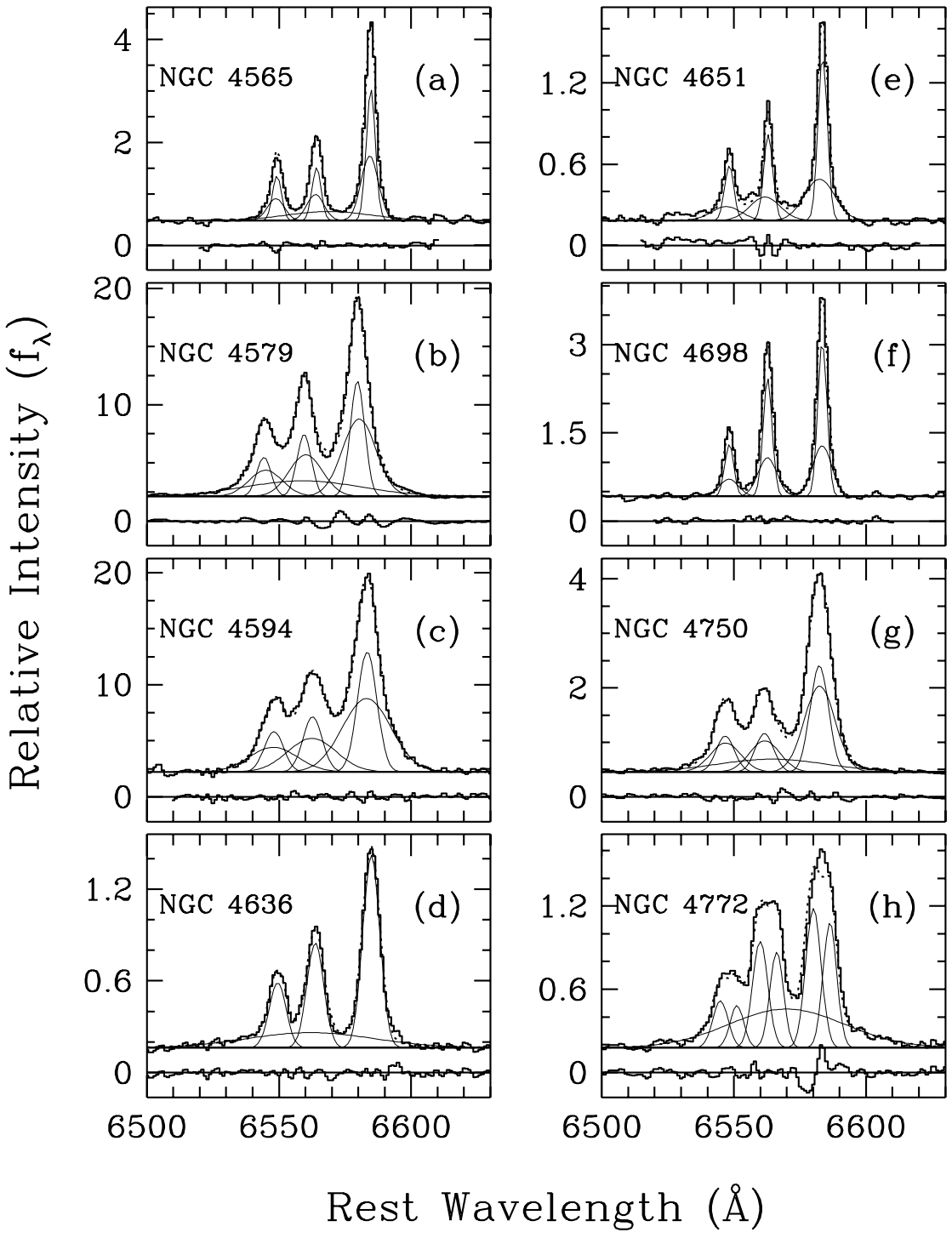


FIG. 13.—Decomposition of the Hα + [N II] region for (*a*) NGC 4565, (*b*) NGC 4579, (*c*) NGC 4594, (*d*) NGC 4636, (*e*) NGC 4651, (*f*) NGC 4698, (*g*) NGC 4750, and (*h*) NGC 4772.

are sufficiently Gaussian in shape that a simple four-component fit is adequate to isolate broad Hα. As with NGC 3031 and NGC 4565, [S II] λ6716 is narrower than [S II] λ6731, indicative of density stratification in the narrow-line region (Filippenko & Sargent 1988).

*NGC 4639.*—This rather prominent Seyfert 1 galaxy had gone unnoticed prior to our survey (Filippenko & Sargent 1986). To better characterize the broad Hα component, we removed the narrow-line contribution using a [S II] model (Fig. 6*f*). The final broad profile (observed on 1985 February 24 UT) has FWHM ≈ 3600 km $s^{-1}$ and FWZI ≈ 9600 km $s^{-1}$; a separate spectrum obtained about a year later showed flux variability at the level of ∼10%. A broad component is seen in Hβ and possibly also in Hγ.

*NGC 4651.*—Although we suspected that broad Hα might be present at a very faint level, we could not confirm its reality unambiguously. In particular, the line profiles of Hα, [N II], and [S II] do not agree in detail, perhaps because

of the difficulty encountered in starlight subtraction for this object. Each of the narrow lines of the H$\alpha$ + [N II] blend was simply fitted with two Gaussians (Fig. 13*e*).

*NGC 4698*.—The emission lines of this low-luminosity Seyfert nucleus are quite narrow (FWHM $\approx$ 170 km s$^{-1}$), despite the fairly early Hubble type (Sa) of the host galaxy. No trace of broad H$\alpha$ is visible in the relatively high S/N spectrum (Fig. 13*f*).

*NGC 4750*.—Broad H$\alpha$ emission definitely exists in this LINER. The high-S/N spectrum reveals faint wings extending well beyond the intrinsic profile of [N II] (Fig. 13*g*). The narrow-line profile obtained from [S II] looks very symmetric.

*NGC 4772*.—Broad H$\alpha$ is present unambiguously, as is evident from the wide base on either side of the [N II] lines (Fig. 13*h*). Unfortunately, undulations in the neighboring continuum compromise the accuracy of the fit to the broad feature. Because of the steep velocity gradient in the inner rotation curve, the narrow lines have a double-peaked or flat-topped profile, which was well reproduced using two Gaussian components derived by fitting the [S II] lines. Although the fit to [N II] $\lambda$6583 shows considerable residuals, we chose to impose stringent constraints because of the complexity of the blend.

*NGC 5005*.—Despite the extremely complicated velocity structure and severe blending of the narrow lines, once again caused by a steep gradient in the inner rotation curve, a rather significant ($f_{\rm blend} \approx 33\%$; Fig. 14*a* broad H$\alpha$ component is suggested if one requires that narrow H$\alpha$ and [N II] have the same profiles as [S II]. The sizable residuals notwithstanding, it is remarkable that such simple constraints can reproduce most of the features of the complex blend.

*NGC 5033*.—The nucleus of NGC 5033 has been detected in X-rays (Halpern & Steiner 1983), and the emission comes from an unresolved source (Koratkar et al. 1995). The very prominent and variable (Paper I) broad H$\alpha$ line, originally noted by Shuder (1980) and Stauffer (1982), can be fitted fairly accurately with a Gaussian of FWHM $\approx$ 2850 km s$^{-1}$ (Fig. 14*b*). The narrow components of H$\alpha$ and [N II], all of which show asymmetric wings, were modeled using the [S II] lines. H$\beta$ also has a visible broad component.

*NGC 5077*.—The derived strength of the broad H$\alpha$ component in this object (Paper I) depends critically on the assumption about the intrinsic [S II] profile, which, unfortunately, is rather uncertain with the present S/N of the spectrum. In particular, different (equally acceptable) assumptions about the [S II] profile can lead to a factor of 3 discrepancy in the final broad H$\alpha$ flux. In Figure 14*c*, we have chosen the set of parameters that gives the smallest probable broad H$\alpha$ flux.

*NGC 5194*.—The broad base of the H$\alpha$ + [N II] blend in NGC 5194 (M51) is predominantly due to the wide, asymmetric wings of the narrow lines. But careful scrutiny reveals that the extremes of the [N II] lines may extend to an FWZI of 6000 km s$^{-1}$ at the faintest flux levels (Fig. 14*d*). Although we cannot formally recover such a weak feature with our line-fitting technique, it is possible that broad H$\alpha$ is present.

*NGC 5273*.—The broad and variable (Stauffer 1982; Paper I) H$\alpha$ emission of the low-luminosity Seyfert 1 nucleus in NGC 5273 (Fig. 6*g*) closely resembles that of NGC 4639 (Fig. 6*f*) in relative strength ($f_{\rm blend} \approx 84\%$) and profile (FWHM $\approx$ 3350 km s$^{-1}$; FWZI $\approx$ 10,000 km s$^{-1}$). As in NGC 4639, soft X-ray emission has been detected from the compact nucleus (Koratkar et al. 1995). The [N II] lines and the narrow component of H$\alpha$ are not well fitted by the model profile derived from [S II], although in this instance the mismatch has an insignificant effect on the measured broad H$\alpha$ flux. Both H$\beta$ and H$\gamma$ also have a broad component.

*NGC 5548*.—This famous Seyfert 1 galaxy has been the target of recent intensive variability monitoring aimed at determining the size and structure of its BLR (see Peterson 1993 for a review). The [S II] lines have FWHM $\approx$ 300 km s$^{-1}$ and display an obvious blue wing. Constraining the narrow H$\alpha$ and [N II] lines to have the same profiles, we subtracted suitably scaled versions of the [S II] profile from the H$\alpha$ + [N II] complex (Fig. 6*h*). The final strengths of the narrow lines, taken such that the broad profile be as smooth as possible at their positions, yield the following narrow-line intensity ratios: ([N II] $\lambda$6583)/H$\alpha$ = 0.9, ([S II] $\lambda\lambda$6716, 6731)/H$\alpha$ = 0.7, ([O I] $\lambda$6300)/H$\alpha$ = 0.4, and ([O III] $\lambda$5007)/H$\beta$ = 10. In addition to the narrow and broad components of H$\alpha$, there is clearly also substantial emission from a distinct component with intermediate velocities (FWHM $\approx$ 1000 km s$^{-1}$). Although the intermediate-width component is much less prominent in H$\beta$, comparison of the profile of [O III] $\lambda$5007 with that of the central peak of H$\beta$ suggests that it might be present. Broad H$\beta$ and H$\gamma$ are present in the blue spectrum, as is an Fe II complex centered near 4550 Å and possibly also He II $\lambda$4686.

*NGC 6500*.—The spectrum of NGC 6500 looks remarkably similar to that of NGC 1052, both in terms of the widths and the relative strengths of the emission lines. But, unlike the case of NGC 1052, our profile decomposition suggests that broad H$\alpha$ emission is absent in NGC 6500 (Fig. 14*e*). A simple two-Gaussian model from [S II] gives an excellent fit to H$\alpha$ and [N II], and the extensions on either side of the blend clearly belong to the intrinsic profile of [N II]. The morphology of the radio continuum emission of NGC 6500 has been interpreted as evidence for a bipolar outflow along the minor axis of the galaxy (Unger, Pedlar, & Hummel 1989), similar in nature to the wind-driven bubbles seen in M82 and NGC 3079 (Heckman, Armus, & Miley 1990; Filippenko & Sargent 1992). The large line widths of the nucleus of NGC 6500 (FWHM $\approx$ 500–600 km s$^{-1}$), however, do not seem to be a direct consequence of the outflow (if indeed present); instead, the two-dimensional spectrum indicates that a steeply rising rotation curve is responsible for the line broadening.

*NGC 6951*.—No broad H$\alpha$ line is found in the Seyfert nucleus of this galaxy (Fig. 14*f*). The emission lines are slightly asymmetric but are well separated at our resolution, and a simple two-component model for the narrow-line profile gives a satisfactory fit to the spectrum.

*NGC 7217*.—As with NGC 5194, the narrow lines have wide wings that account for most of the broad base of the H$\alpha$ + [N II] blend (Fig. 14*g*). However, an extremely weak component of broad H$\alpha$ may be present, as suggested by the very faint wings on either end of [N II]. Spectra of higher S/N are necessary to confirm this.

*NGC 7479*.—The velocity structure of NGC 7479 (Fig. 14*h*) is reminiscent of that of NGC 3245 (Fig. 10*b*), except that in this case the narrow lines have a prominent blue asymmetry. Note that H$\alpha$ and [N II] have slightly different profiles, reflecting differences in the [N II]/H$\alpha$ ratio between

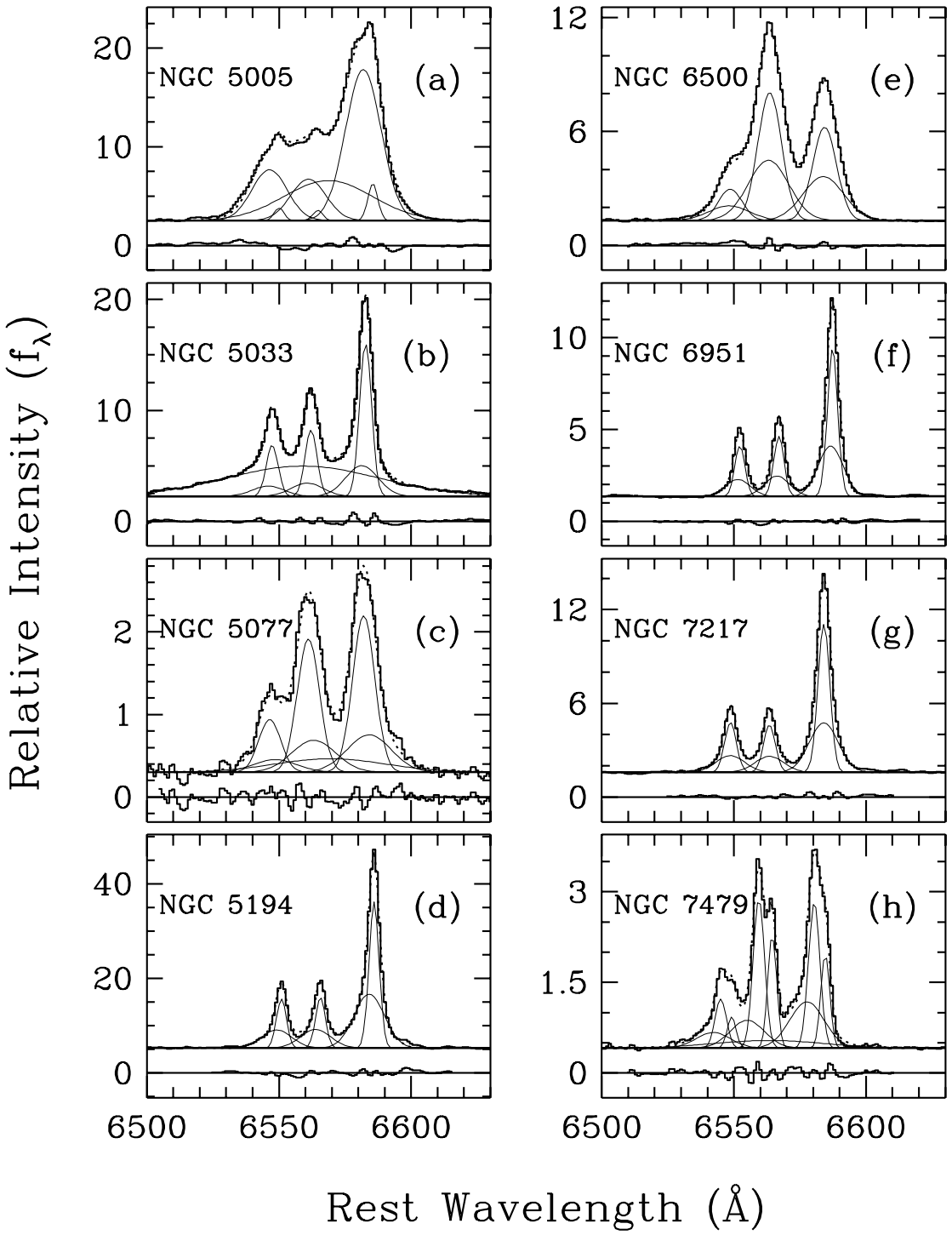


FIG. 14.—Decomposition of the Hα + [N II] region for (*a*) NGC 5005, (*b*) NGC 5033, (*c*) NGC 5077, (*d*) NGC 5194, (*e*) NGC 6500, (*f*) NGC 6951, (*g*) NGC 7217, and (*h*) NGC 7479.

the two main velocity components of the line. Extremely faint wings, amounting to only ~8% of the flux of the Hα + [N II] blend, can be seen with FWZI ≈ 3700 km s$^{-1}$.

*Special cases.*—A broad base (FWHM ≈ 1500–2000 km s$^{-1}$) sometimes accompanies the Hα line in galaxies whose spectrum is dominated by emission from Wolf-Rayet stars (so-called Wolf-Rayet galaxies). One such object, discussed by Sargent & Filippenko (1991), is NGC 4214, and several other examples found in our survey (IC 10, NGC 1156, NGC 1569, NGC 4532) were noted in Paper II. We do not include these cases in our overall statistics of broad Hα emission (§ 4), since in this paper we are only concerned with emission arising from AGNs.

## 4. SURVEY STATISTICS AND CONCLUSIONS

An optical spectroscopic survey specifically designed to detect low-luminosity AGNs has recently been completed. This paper presents the data for the subset of nuclei showing definite or probable evidence of broad Hα emission, similar in character to, but much weaker in strength

than, that of more luminous type 1 Seyferts. The overall statistics of the survey can be summarized as follows: of the 211 emission-line nuclei classified as LINERs, transition objects (composite H II nucleus/LINER), or Seyferts (see Paper III for classification of all objects), 34 (16%) definitely have broad Hα, and an additional 12 (6%) probably do. Questionable detections were found for another 18 objects (Table 2), while 27 objects suspected to have broad Hα based on visual inspection turned out to yield negative results (Table 3). Thus, approximately 20% of all nearby AGNs, corresponding to ~10% of all nearby, bright ($B_T \leq$ 12.5 mag) galaxies, can be considered to be AGNs harboring a BLR ("type 1" objects). Of the 34 objects with definite detections of broad Hα, only nine are well-known Seyfert 1 galaxies (Véron-Cetty & Véron 1996). The majority have substantially lower Hα luminosities, and many of the detections or probable detections described in this paper are reported for the first time. Although the presence of broad Hα emission was previously suspected in a number of objects, quantitative measurements were lacking. As demonstrated in § 3, in most instances the detection of broad Hα and subsequent determination of its line parameters require data of extremely high quality, sufficient spectral resolution, careful treatment of starlight contamination, and meticulous profile decomposition.

Excluding all the previously recognized (Véron-Cetty & Véron 1996) Seyfert 1 nuclei (retaining only NGC 4395), the broad Hα lines of the remaining objects have typical luminosities of $\sim 10^{39}$ ergs $s^{-1}$ and FWHMs of 2200 km $s^{-1}$ and constitute 10%–50% of the Hα + [N II] blend. Five sources have broad Hα luminosities of only (1–3) × $10^{38}$ ergs $s^{-1}$. The lowest luminosity source with a probable detection is the nucleus of NGC 4565, having a broad Hα luminosity of only 8 × $10^{37}$ ergs $s^{-1}$. The luminosity function of the sources described in this study will be considered in a forthcoming paper.

TABLE 2

AMBIGUOUS CASES

| Galaxy | Class[a] |
|---|---|
| NGC 660 | T2: |
| NGC 1358 | S2 |
| NGC 2273 | S2 |
| NGC 2655 | S2 |
| NGC 2685 | S2: |
| NGC 2841 | L2 |
| NGC 3079 | S2 |
| NGC 3245 | T2: |
| NGC 3898 | T2 |
| NGC 4419 | T2 |
| NGC 4486 | L2 |
| NGC 4501 | S2 |
| NGC 4651 | L2 |
| NGC 5194 | S2 |
| NGC 5363 | L2 |
| NGC 5846 | T2: |
| NGC 5866 | T2 |
| NGC 7217 | L2 |

[a] Classification of nucleus (see Paper III), where L = LINER, T = transition object (LINER/H II nucleus), S = Seyfert, 1 = type 1 and 2 = type 2. Entries followed by a colon denote uncertain or ambiguous classification of the narrow-line spectrum.

TABLE 3

NULL DETECTIONS[a]

| Galaxy | Class[b] |
|---|---|
| NGC 410 | T2: |
| NGC 1167 | S2 |
| NGC 1667 | S2 |
| NGC 1961 | L2 |
| NGC 2768 | L2 |
| NGC 2911 | L2 |
| NGC 3166 | L2 |
| NGC 3190 | L2 |
| NGC 3486 | S2 |
| NGC 3507 | L2 |
| NGC 3945 | L2 |
| NGC 3976 | S2: |
| NGC 4192 | T2 |
| NGC 4261 | L2 |
| NGC 4314 | L2 |
| NGC 4321 | T2 |
| NGC 4457 | L2 |
| NGC 4552 | T2: |
| NGC 4589 | L2 |
| NGC 4594 | L2 |
| NGC 4698 | S2 |
| NGC 5985 | L2 |
| NGC 6340 | L2 |
| NGC 6500 | L2 |
| NGC 6951 | S2 |
| NGC 7742 | T2 |
| NGC 7743 | S2 |

[a] Obvious visual null detections not listed.

[b] Classification of nucleus (see Paper III), where L = LINER, T = transition object (LINER/H II nucleus), S = Seyfert, 1 = type 1 and 2 = type 2. Entries followed by a colon denote uncertain or ambiguous classification of the narrow-line spectrum.

Of the 46 objects with broad Hα emission, more than half belong to the LINER category (22 LINERs and 2 transition objects). In the context of trying to decipher the physical origin of this class of objects and to establish their relationship to Seyfert nuclei, this is an important finding. It implies that LINERs, like Seyferts, evidently come in two flavors—some have a visible BLR, and others do not. By direct analogy with the nomenclature established for Seyferts, we proposed in Paper III that the "type 1" and "type 2" designations be extended to include LINERs and transition objects.

The broad Hα detection rates reported here represent lower limits to the true incidence of broad line–emitting regions in the sample objects. It should be clear from the examples given in § 3 that ambiguities concerning the reality of the lines are encountered in some instances, and, from our discussion of the likely systematic errors (§ 2.4), there is a practical limit to which a weak, broad spectral feature can be extracted from the integrated spectra. Detecting the broad line may be especially challenging in AGNs whose integrated spectrum is heavily contaminated by emission from nearby H II regions. In such cases, we anticipate the AGN component, including any possible BLR emission, to be substantially diluted. This may explain why broad Hα was detected in so few of the transition objects (only two out of 65 sources; see Paper V) compared with the LINERs (22 out of 94 sources) or the Seyferts (22 out of 52

sources). Thus, although our survey for broad Hα emission is the most comprehensive and sensitive search of its kind, it should not be regarded as "complete." To significantly improve the sensitivity to even weaker emission would require observations at much higher spatial resolution, in order to better isolate the nucleus from the contaminating bulge starlight. The superior image quality of *HST*, especially in conjunction with the use of small apertures, should be especially useful in this regard. As a concrete illustration of the advantages to be gained, we note that Kormendy et al. (1997) discovered a broad component of Hα in their recent *HST* spectra of NGC 4594, whereas we could not detect it in our ground-based data (§ 3). Thus a concerted spectroscopic follow-up program using the *HST* would be of considerable value in ascertaining the completeness of our ground-based survey.

The research of L. C. H. is currently funded by a postdoctoral fellowship from the Harvard-Smithsonian Center for Astrophysics. Financial support for this work was provided by NSF grants AST 89-57063 and AST 92-21365, by NASA grant NAG 5-3556, and by NASA grants AR-5291-93A and AR-5792-94A from the Space Telescope Science Institute (operated by AURA, Inc., under NASA contract NAS 5-26555). We thank Chris McKee and Hy Spinrad for their critical reading of an earlier draft of the manuscript, and an anonymous referee for suggesting some points of clarification.

## REFERENCES

Abell, G. O., Eastmond, T. S., & Jenner, D. C. 1978, ApJ, 221, L1
Alloin, D., Pelat, D., Boksenberg, A., & Sargent, W. L. W. 1983, ApJ, 275, 493
Antonucci, R. R. J., & Miller, J. S. 1985, ApJ, 297, 621
Bahcall, J. N., Kirhakos, S., Saxe, D. H., & Schneider, D. P. 1997, ApJ, 479, 642
Baldwin, J. A., Wilson, A. S., & Whittle, M. 1987, ApJ, 319, 84
Balick, B., & Heckman, T. M. 1983, ApJ, 265, L1
Barth, A. J., Reichert, G. A., Filippenko, A. V., Ho, L. C., Shields, J. C., Mushotzky, R. F., & Puchnarewicz, E. M. 1996, AJ, 112, 1829
Bietenholz, M., et al. 1996, ApJ, 457, 604
Blackman, C. P., Wilson, A. S., & Ward, M. J. 1983, MNRAS, 202, 1001
Boksenberg, A., & Netzer, H. 1977, ApJ, 212, 37
Boroson, T. A., Oke, J. B., & Green, R. F. 1982, ApJ, 263, 32
Boyce, P. J., et al. 1996, ApJ, 473, 760
Caganoff, S., et al. 1991, ApJ, 377, L9
Cecil, G., Bland, J., & Tully, R. B. 1990, ApJ, 355, 70
De Robertis, M. M., & Osterbrock, D. E. 1986, ApJ, 301, 727
Ferrarese, L., Ford, H. C., & Jaffe, W. 1996, ApJ, 470, 444
Filippenko, A. V. 1985, ApJ, 289, 475
———. 1989, in Active Galactic Nuclei, ed. D. E. Osterbrock & J. S. Miller (Dordrecht: Kluwer), 495
———. 1996, in ASP Conf. Proc. 103, The Physics of LINERs in View of Recent Observations, ed. M. Eracleous et al. (San Francisco: ASP), 17
Filippenko, A. V., & Halpern, J. P. 1984, ApJ, 285, 458
Filippenko, A. V., & Ho, L. C. 1997, ApJ, submitted
Filippenko, A. V., Ho, L. C., & Sargent, W. L. W. 1993, ApJ, 410, L75
Filippenko, A. V., & Sargent, W. L. W. 1985, ApJS, 57, 503 (Paper I)
———. 1986, in Structure and Evolution of Active Galactic Nuclei, ed. G. Giuricin et al. (Dordrecht: Reidel), 21
———. 1988, ApJ, 324, 134
———. 1989, ApJ, 342, L11
———. 1992, AJ, 103, 28
Fosbury, R. A. E., Melbold, U., Goss, W. M., & Dopita, M. A. 1978, MNRAS, 183, 549
Giovannini, G., Feretti, L., & Comoretto, G. 1989, ApJ, 358, 159
Greenhill, L. J., Jiang, D. R., Moran, J. M., Reid, M. J., Lo, K.-Y., & Claussen, M. J. 1995, ApJ, 440, 619
Halpern, J. P., & Steiner, J. E. 1983, ApJ, 269, L37
Harms, R. J., et al. 1995, ApJ, 435, L35
Heckman, T. M. 1980, A&A, 87, 152
Heckman, T. M., Armus, L., & Miley, G. K. 1990, ApJS, 74, 833
Heckman, T. M., Balick, B., & Crane, P. C. 1980, A&AS, 40, 295
Ho, L. C. 1995, Ph.D. thesis, Univ. California, Berkeley
———. 1996, in ASP Conf. Proc. 103, The Physics of LINERs in View of Recent Observations, ed. M. Eracleous et al. (San Francisco: ASP), 103
Ho, L. C., Filippenko, A. V., & Sargent, W. L. W. 1993, ApJ, 417, 63
———. 1994, in IAU Symp. 159, Multiwavelength Continuum Emission of AGN, ed. T. J.-L. Courvoisier & A. Blecha (Dordrecht: Reidel), 275
———. 1995, ApJS, 98, 477 (Paper II)
———. 1996, ApJ, 462, 183
———. 1997a, ApJS, 112, 315 (Paper III)
———. 1997b, ApJ, 487, 568 in press (Paper V)
Huchra, J. P., Wyatt, W. F., & Davis, M. 1982, AJ, 87, 1628
Ishisaki, Y., et al. 1996, PASJ, 48, 237
Jaffe, W., Ford, H. C., Ferrarese, L., van den Bosch, F., & O'Connell, R. W. 1993, Nature, 364, 213
———. 1996, ApJ, 460, 214
Kaspi, S., et al. 1996, ApJ, 470, 336
Keel, W. C. 1983, ApJ, 269, 466
Keel, W. C., & Miller, J. S. 1983, ApJ, 266, L89
Khachikian, E. Y., & Weedman, D. W. 1974, ApJ, 192, 581
Koratkar, A. P., Deustua, S., Heckman, T. M., Filippenko, A. V., Ho, L. C., & Rao, M. 1995, ApJ, 440, 132
Kormendy, J., et al. 1997, ApJ, 473, L91
Malkan, M. A., & Filippenko, A. V. 1983, ApJ, 275, 477
Malkan, M. A., Margon, B., & Chanan, G. A. 1984, ApJ, 280, 66
Maoz, D., et al. 1991, ApJ, 367, 493
McLeod, K. K., & Rieke, G. H. 1994a, ApJ, 420, 58
———. 1994b, ApJ, 431, 137
Miller, J. S., Goodrich, R. W., & Mathews, W. G. 1991, ApJ, 378, 47
Miller, J. S., Tran, H., & Sheinis, A. 1996, BAAS, 28, 1301
Miyoshi, M., et al. 1995, Nature, 373, 127
Netzer, H. 1990, in Active Galactic Nuclei, SAAS-FEE Advanced Course 20, Swiss Society for Astrophysics and Astronomy, ed. T. J.-L. Courvoisier & M. Mayor (Berlin: Springer), 57
Osterbrock, D. E. 1981, ApJ, 249, 462
Osterbrock, D. E., & Pogge, R. W. 1985, ApJ, 297, 166
Peimbert, M., & Torres-Peimbert, S. 1981, ApJ, 245, 845
Pelat, D., & Alloin, D. 1980, A&A, 81, 172
Peterson, B. M. 1993, PASP, 105, 247
Petre, R., Mushotzky, R. F., Serlemitsos, P. J., Jahoda, K., & Marshall, F. E. 1993, ApJ, 418, 644
Phillips, M. M., & Malin, D. F. 1982, MNRAS, 199, 905
Reichert, G. A., Branduardi-Raymont, G., Filippenko, A. V., Mason, K. O., Puchnarewicz, E. M., & Wu, C.-C. 1992, ApJ, 387, 536
Rose, J. A., & Tripicco, M. J. 1984, ApJ, 285, 55
Sandage, A. R., & Tammann, G. A. 1981, A Revised Shapley-Ames Catalog of Bright Galaxies (Washington: Carnegie Inst. Washington)
Sargent, W. L. W., & Filippenko, A. V. 1991, AJ, 102, 107
Schmidt, M., & Green, R. F. 1983, ApJ, 269, 352
Shields, G. A., & Oke, J. B. 1975, ApJ, 197, 5
Shields, J. C., & Filippenko, A. V. 1988, ApJ, 332, L55
———. 1990, AJ, 100, 1034
———. 1996, A&A, 311, 393
Shuder, J. M. 1980, ApJ, 240, 32
Shuder, J. M., & Osterbrock, D. E. 1981, ApJ, 250, 55
Stauffer, J. R. 1982, ApJ, 262, 66
Stüwe, J. A., Schulz, H., & Hühnermann, H. 1992, A&A, 261, 382
Tully, R. B. 1988, Nearby Galaxies Catalog (Cambridge: Cambridge Univ. Press)
Unger, S. W., Pedlar, A., & Hummel, E. 1989, A&A, 208, 14
Veilleux, S. 1991, ApJS, 75, 357
Veilleux, S., Cecil, G., Bland-Hawthorn, J., Tully, R. B., Filippenko, A. V., & Sargent, W. L. W. 1994, ApJ, 433, 48
Véron, P. 1979, A&A, 78, 46
Véron-Cetty, M.-P., & Véron, P. 1996, A Catalog of Quasars and Active Nuclei (ESO Sci. Rep. 17) (7th ed; Garching: ESO)
Walker, M. F. 1968, ApJ, 151, 71
Weedman, D. W. 1976, ApJ, 208, 30
Wilkes, B. J., Schmidt, G. D., Smith, P. S., Mathur, S., & McLeod, K. K. 1996, ApJ, 455, L13
Winge, C., Peterson, B. M., Horne, K., Pogge, R. W., Pastoriza, M. G., & Storchi-Bergmann, T. 1995, ApJ, 445, 680
Wyckoff, S., Wehinger, P. A., Spinrad, H., & Boksenberg, A. 1980, ApJ, 240, 25